ISA Transactions 158 (2025) 452–467

Contents lists available at ScienceDirect

ISA Transactions

journal homepage: www.elsevier.com/locate/isatrans

Research article

Noninteracting optimal and adaptive torque control using an online parameter estimation with help of polynomials in EKF for a PMSM

Tanja Zwerger [a], Paolo Mercorelli [b,*]

[a] Rolls Royce Power Systems GmbH, Maybachplatz 1, 88045 Friedrichshafen, Germany
[b] Leuphana University of Lueneburg, Universitaetsallee 1, 21335 Lueneburg, Germany

ARTICLE INFO

Keywords:
Torque control in PMSM
Extended Kalman filter
Parameter estimation
Univariate polynomial
Noninteracting control

ABSTRACT

This paper addresses a non-interacting torque control strategy to decouple the d- and q-axis dynamics of a permanent magnet synchronous machine (PMSM). The maximum torque per ampere (MTPA) method is used to determine the reference currents for the desired torque. To realize the noninteracting control, knowledge concerning the inductances L_d and L_q of the electrical machine is necessary. These two inductances are estimated by two extended Kalman filters (EKFs), which use a univariate polynomial as a model to describe the saturation effects of the PMSM. The Kalman filters (KF) are realized within a noninteracting control system to improve the observability of the inductance. Despite the non-perfect decoupling, thanks to the structural stochastic nature of the KFs, noninteracting cancellation errors are represented with its process noise and the inductances are estimated sufficiently well. In this sense, we can speak about KFs for and within noninteracting control. Estimating inductances is fundamental for optimal torque control, which is a viable approach to reducing mechanical vibration and disturbance. Moreover, the control strategy of model-based techniques must be adaptively tuned to work properly. Starting from the existing literature, a viable control structure is proposed in which the stability of the control loop using a Proportional Integral (PI) controller is shown for the resulting time-varying system. In fact, the model is represented as a time-varying system because of the presence of the variable inductances L_d and L_q and because of the presence of the velocity of the rotor which is not considered as a state. In this paper, a forward Euler discretization is used to realize the observer in the discrete experimental setup. Measures realized with hardware in the loop (HIL) show interesting results in the context of inductance estimation, due to the advantage of the reduction of the dimensions of the two decoupled EKFs resulting from the noninteraction control. Using the HIL simulator, the proposed torque control strategy is investigated, showing promising results in terms of increasing observability due to decoupling. This and the usage of univariate polynomials in EKF calculations lead to significant reduction of measurement points, reduction of oscillations and ripples, deviation between desired and achieved torque and reduction of disturbances. Moreover, the proposed control strategy using a very limited calculation load, at the same time, maintains the ripples inside the technical limits of the obtained torque. Both effects are due to the decoupled EKFs with simplified and reduced order of the models using univariate polynomials, which require significantly fewer measuring points in the run-up to the creation of the model of the inductances L_d and L_q.

1. Introduction

Permanent magnet synchronous machines (PMSMs) are increasingly used for applications with limited space and high power density requirements, especially in high torque demanding applications. PMSMs are therefore a welcome addition in determining a suitable electric drive, and not only in the automotive sector, where the increasing importance of electromobility is becoming ever clearer. The modern control techniques for electrical motors are model based ones and are often combined with sensorless control strategies to reduce the number of sensors. Estimation of the state, parameters and disturbances are essential for the accuracy of the control of a PMSM in optimal tracking, especially for PMSMs with a high reluctance torque. A good overview of the influence in flux weakening capability for different geometric approaches is given in [1]. Maximum torque per ampere

* Corresponding author.
E-mail addresses: Tanja.Zwerger@stud.leuphana.de (T. Zwerger), paolo.mercorelli@leuphana.de (P. Mercorelli).

https://doi.org/10.1016/j.isatra.2024.12.037
Received 9 June 2023; Received in revised form 22 December 2024; Accepted 22 December 2024
Available online 1 January 2025

The main nomenclature

$u_d(t)$	Direct voltage input
$u_q(t)$	Quadrature voltage input
$i_d(t)$	Direct current
$i_q(t)$	Quadrature current
$i_{dd}(t)$	Desired direct current
$i_{qd}(t)$	Desired quadrature current
$\omega_r(t)$	Mechanical angular velocity of the rotor
$\omega_{el}(t) = p\omega_r(t)$	Electrical rotor angular velocity
p	Pole pair number
R_s	Coil resistance
$L_d(t)$	Direct axis self-inductance
$L_q(t)$	Quadrature axis self-inductance
Ψ_p	Main flux constant
$\psi_d(t)$	Direct flux component
$\psi_q(t)$	Quadrature flux component
$T(t)$	Torque
Θ_d	Coefficient polynomial for L_d calculation
Θ_q	Coefficient polynomial for L_q calculation
$\theta_r(t)$	Mechanical angle of the rotor
$\theta_{el}(t)$	Electrical angle of the rotor
λ	Eigenvalues of the desired electrical system
$F(\omega_r(t))$	Matrix of eigenvalues
u_{ff}	Voltage feedforward action
$\Delta_{d/q}$	Time-varying cancellation errors
$\Delta_{L_{d/q}}$	Cancellation errors in inductance
Δ_{ff}	Cancellation errors in feedforward action
$v_{d/q}(t)$	Supplementary inputs of the system
$K_{pd/pq}$	Parameters of proportional control
$K_{Id/Iq}$	Parameters of integral control

(MTPA) control is a rather complex control strategy which aims to operate the motor as energy-efficiently as possible and is based on the approach of achieving the maximum torque from the available current.

1.1. MTPA in an outer control loop

The MTPA control runs in an outer control loop and defines the desired current input for the current control, which is calculated out of the desired torque. The MTPA approach makes it possible to calculate the desired torque with the smallest possible desired currents i_{dd} and i_{qd} and thus solves the optimization problem according to Lagrange. The advantage is that the copper losses, which occur mainly in the constant torque range of a PMSM and are largely caused by the impressed current, can be reduced as a result. For the MTPA approach and the feedforward action in control, an exact knowledge of the parameter maps is necessary, among other things, to avoid demagnetization due to the incorrect current supply, as described in [2]. In [2] a new method to detect the demagnetization is proposed. In order to avoid demagnetization, the use of MTPA with its optimal structure when the inductance is estimated is a possible measure to prevent this effect.

1.2. Parameter estimation in PMSM control: state of the art

Therefore, in [3] a machine model is introduced which allows the consideration of temperature and saturation effects. To estimate the state of a system, an extended Kalman filter (EKF) is often used, like it is shown in [4]. In the field of synchronous machines, different contributions appeared recently, e.g. [5,6] in which a comparison between EKFs and sliding mode observers is proposed in the presence of measurement noise. Recently, through a sensitivity analysis, the contributions [7,8] investigated the influence of model uncertainty on the observed position and the robustness of a Proportional Integral (PI) observer in current control of PMSM drives. In [9] the speed regulation of a PMSM is investigated and the key role of a disturbance observer in the context of the control is pointed out. In particular, it is to notice an increasing interest in sensorless control strategy for PMSMs, see [10]. When emphasizing the topic of the optimal control, for example [11] can be taken into account, where a stabilization problem is solved based on a design of a special feedback function. In [12], and very recently in [13,14], different observers for the sensorless control of PMSMs with online resistance and inductance estimation are proposed. In particular in [12] the author proposes a position observer and a velocity estimator for a non-linear actuator for motor applications. This is realized by combining both in a cascade structure. In [13] the investigation elaborates a novel online full parameter estimation method for PMSMs. In the $d-q$ frame, the inductance parameters can only be estimated in the transient phase, whereas in the α-β frame, the inductance parameters can also be estimated in the steady state and in the transient state. The authors in [14] show a modified conventional flux-sliding mode observer which is considered using the motor parameter variations. An embedded flux observer is thereby constructed to replace the conventional phase locked loop for estimating the velocity and position in the sensorless PMSM control system. More specifically, contributions such as [8] investigate the influence of model uncertainty on the observed position and the robustness of an observer in current control of PMSM drives. Concerning the analysis of the observability, the contributions in [15–17] showed that the PMSM system in stator-fixed α,β-coordinates is observable with respect to the states i_α, i_β, ω_{el}, θ_{el} using only measurements of the currents $i_{\alpha,\beta}$, as long as the velocity ω_{el} is not zero or $L_d \neq L_q$. The estimation of the inductance in the presence of saturation is not easy to carry out, since it is a non-linear progression of the quantities to be estimated for the control of the PMSM. The analysis of saturations and their estimation represent, in accordance with the current literature, several problems in mechatronic systems and their control. In fact, in [18] a pre-action control strategy is proposed to avoid magnetic saturation in a U-magnet system for automotive applications. In [19] a Lyapunov based control strategy is used to control an actuator also in the presence of saturation. Contributions as [20] and, more recently, in [21–24] show that sensorless control strategies are a promising approach for innovative control strategies in mechatronic contexts. More in depth, in [21], the conception, design, and implementation of a discrete extended Kalman filter and a Takagi–Sugeno observer are proposed. A comparison of the performance and the calculation load is shown. The authors in [22] propose a developed direct torque control strategy for the torque ripple mitigation, in which a current-sensing scheme with fewer current sensors is presented. In [23] a position estimation method based on current injection of the idle phase is shown. In [25–27] and more recently in [28], different conditions are considered to estimate the parameters of the machine. To go more in depth, in [25] a method to accommodate the changes in the magnetic flux and the inductances with the level of saturation is proposed. The authors in [26] analyze the motor characteristics with the help of equivalent circuit diagrams, the inductance and the iron loss resistance, which are influenced by the magnetic saturation, are determined with the help of static finite element analysis. In [27] a model-reference-based online identification method is proposed to estimate PMSM parameters. It is shown that all parameters are not identifiable in steady state and a choice of these parameters to be estimated has to be made according to the objectives. The estimation of the inductances is a prior problem for the control of PMSM. Therefore, in [29], a compensation method of a position estimation error for a high-speed surface-mounted PMSM based on a robust inductance estimation is proposed. For the estimation of the inductance, the authors in [30] provide a solution with the estimation of an additional saturation factor by using a recursive least

squares (RLS) method. The estimated saturation factor is subtracted from the estimated nominal inductance. A promising future approach is described in [31], in which the authors propose and promote the accuracy of the model parameter identification using fractional model approach of the nonlinearities of the PMSM.

1.3. Contribution and highlights

However, the solution proposed in this contribution assumes, in accordance with the measured data of the considered electric machine, that the quadrature inductance L_q strongly depends on the quadrature current i_q and that the direct inductance L_d depends on the direct current i_d. But, according to [25], an increasing negative current i_d desaturates the d-inductance, while an increasing positive i_q current leads to saturation of the same iron. This leads to a constant behavior of the d-inductance in a certain range until the q-current increases above a certain value where the d-inductance decreases due to the resulting saturation. This is the reason why the usually higher self-saturation effect for the d-inductance can be much smaller in case of driving with a negative current i_d. If an optimal desired ratio between a positive current i_q and a negative current i_d are precalculated using MTPA as reference currents for control, a lower self-saturation effect in the L_d inductance is obtained. For this reason, the proposed method in this paper provides a solution by calculating a polynomial, like in [32], where the dependency of L_d and L_q on the quadrature current i_q is taken into account. The resulting usage of the univariate polynomial for calculating the model of the two decoupled EKFs is therefore less complex and needs less measurement points, what is a big advantage, especially if the measurement is not or only to a limited amount possible. This is the case, for example, if the electrical machine to be measured has already been applied and is therefore coupled to the load. To control the system a noninteracting strategy is adopted to decouple the electrical dynamics of the machine. To make the proposed noninteracting control strategy more robust, the estimation of L_d and L_q in the presence of saturation is needed. In order to achieve the estimation of these parameters, two EKFs are used for the estimation of L_d and L_q of the decoupled system. The two decoupled EKFs can be set up with much smaller matrices, what is beneficial in regards to their observability level or in terms of observability quality to stay with the terminology of [33,34]. Another approach for the control in saturated conditions is shown in [35], where a bivariate polynomial together with a combined Kalman filter is taken into account for estimating the nonlinear and current dependent states of the inductances. As the bivariate polynomial is able to consider current dependency of the inductances in both, d- and q-, directions, the accuracy of the model increases. The disadvantage is, that the calculation of the polynomial is getting more complex and the Kalman filter equations are growing. The measurements which have to be done for the PMSM before the polynomial can be calculated go ahead with more effort. When it comes to a comparison of the sampling times, [36] gives an explanation, why a backward Euler calculation for the Kalman filter is beneficial. Especially for smaller digital signal processors (DSPs), where smaller sampling times are not possible due to higher calculation loads, a backward Euler approach is a good example how this issue can be solved. Again, the disadvantage of the high complexity of the EKF equations has to be considered. A very good overview of possibilities how to control a PMSM is given in [37]. The topic of estimation principles is shown here, but only non-saturated states for invariable inductances of electrical machines are considered, the estimations of saturated inductances is let out as an open problem. In [13], observability is demonstrated using α-β transformation before the parameters are estimated with help of RLS method. Compared to this paper, the results presented here with EKF are advanced, as the EKF gives a more precise estimation method. As a rule, however, using EKF approach in general, this advantage is paid by an increase in computational intensity. In the underlying contribution, however, this disadvantage is eliminated by using two decoupled EKFs with smaller matrices, thus significantly reducing the computational load. Estimation of the parameters L_d and L_q are of fundamental importance in the use of MTPA control strategy to obtain an accurate optimality of the reference currents i_d and i_q. Setting an appropriate optimal control represents a fundamental issue for reduction of mechanical oscillations and disturbances, [38] and maintain, at the same time, ripples inside the technical limits in the obtained torque, see [39]. In general, to design control to restrain ripples is a fundamental issue in PMSM, see [40]. Optimal control strategies are model based approaches which need to be adaptively tuned to work properly, see [41]. As already explained, the estimation of the inductances is based on an EKF which is an algorithm widely used in control of mechanical systems, see [42] in particular for uncertainties identification to improve the mechanical performances, see [43]. Starting from the existing literature, see [44], a viable control structure is proposed in which the stability of the control loop using a PI controller is also shown for the resulting time-varying system. In fact, the model is represented as a time-varying system because of the presence of the variable inductances L_d and L_q and because of the presence of the velocity of the rotor which is not considered as a state. In Fig. 1 the complete schematic control structure, including of the estimation with help of the EKFs, is shown. The current control is set up by PI controller. To summarize the tasks, this work deals with

- setting an appropriate optimal control strategy which represents a fundamental issue for reduction of torque ripple and disturbances and bias between desired and obtained torque. Moreover, the observability quality is increased due to the decoupling noninteraction control and thus helps to increase the quality of the estimated non measurable states L_d and L_q. Measurements, based on hardware in the loop (HIL), validate the proposed torque control strategy showing promising results in terms of an increased observability quality;
- estimation of the inductance L_d and L_q of a PMSM through two decoupled EKFs, which in particular advances the results obtained with an RLS as proposed recently in [30];
- a resulting control scheme consisting of an inner noninteracting adaptive control loop realized through the adaptation of the estimated inductance to show that the realized EKFs are em for and within a noninteracting control which represents an emerging topic in power electronics, see recent literature, for example in [45];
- noninteracting cancellation errors due to the non perfect knowledge of the system will be stochastically included and represented in the process noise of the two corresponding EKFs.
- in terms of PI controller, moving from [44] in which a PI controller is considered, but saturation and estimation of L_d and L_q are not taken into account, in this paper a viable control structure is proposed in which the stability of the control loop using a PI controller is also shown for the resulting time-varying system.
- methodological contribution in terms of observability with respect to [33,34,46].

In general, the online identification of inductances is an important topic in power electronics, as the further development of already consolidated technologies in literature proves, see [47]. The advantage is the estimation with small matrices in the EKF due to decoupling by the backtracked estimated inductance. This means that the usually high computational effort of the EKF can be drastically reduced combined with an improvement of the observability and thus leads to an improvement in the estimation of the parameters.

1.4. Structure of the paper

The paper is organized in the following way: Section 2 is dedicated to the description of the physical system; in Section 3 the calculations of the univariate polynomials are shown; Section 4 is devoted to the

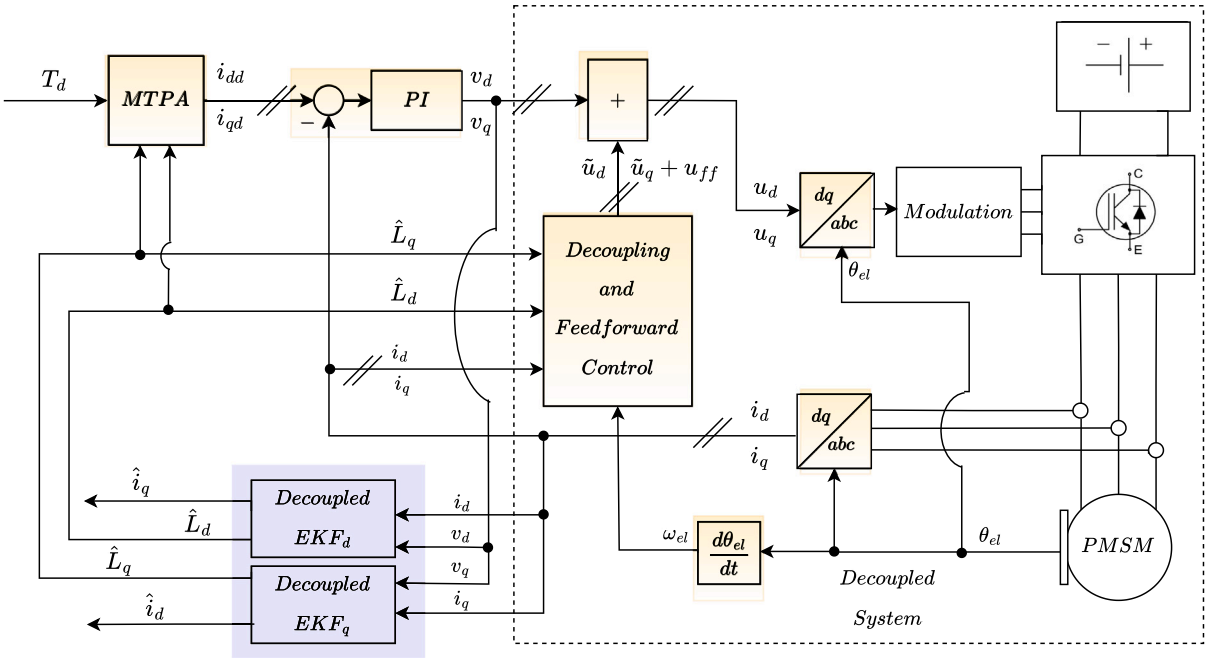

Fig. 1. Schematic control structure: the controller and observer parts are indicated in yellow and blue respectively. (For interpretation of the references to color in this figure legend, the reader is referred to the web version of this article.)

realization of the noninteracting control structure and its robustification using a decoupling controller together with PI control; Section 5 shows how the EKF is conceived; the main contribution is given by the measurement and results in Section 6 together with a following "Discussion and analysis" in Section 7. In the "Discussion and analysis" Section, some particular issues, such as limitations of the contribution, polynomial approximation, observability analysis are examined and analyzed. A conclusion part closes the paper. At the end, in an Appendix, some particular issues regarding Kalman equations and convergence of the proposed observer are presented.

2. Description of the physical system

The field-oriented control is the most common control technique for a PMSM. The observation of instantaneous values takes place in a rotor-oriented reference system. Therefore, a dq-model, which is developed from the three-phase PMSM model is set up by help of the Clarke–Park transformation. The equations which are obtained for the currents i_d and i_q are written in (1) and (2) for variables L_d and L_q.

$$\frac{di_d(t)}{dt} = \frac{u_d(t)}{L_d(t)} - \frac{i_d(t)R_s}{L_d(t)} + \frac{\omega_{el}(t)L_q(t)i_q(t)}{L_d(t)}. \tag{1}$$

$$\frac{di_q(t)}{dt} = \frac{u_q(t)}{L_q(t)} - \frac{i_q(t)R_s}{L_q(t)} - \frac{\omega_{el}(t)L_d(t)i_d(t)}{L_q(t)} - \frac{\omega_{el}(t)\Psi_p}{L_q(t)}. \tag{2}$$

The electrical equations for the voltages are obtained in (3) and (4):

$$u_d(t) = i_d(t)R_s + \frac{d\psi_d(t)}{dt} - \omega_{el}(t)\psi_q(t). \tag{3}$$

$$u_q(t) = i_q(t)R_s + \frac{d\psi_q(t)}{dt} + \omega_{el}(t)\psi_d(t). \tag{4}$$

The physical model of the PMSM, in which because of the velocity ω_r is not a state variable, can also be presented as a time-varying system as follows:

$$\begin{bmatrix} \frac{di_d(t)}{dt} \\ \frac{di_q(t)}{dt} \end{bmatrix} = \underbrace{\begin{bmatrix} \frac{-R_s}{L_d(t)} & \frac{L_q(t)}{L_d(t)}p\omega_r(t) \\ -\frac{L_d(t)}{L_q(t)}p\omega_r(t) & \frac{-R_s}{L_q(t)} \end{bmatrix}}_{A(t)} \begin{bmatrix} i_d(t) \\ i_q(t) \end{bmatrix} + \underbrace{\begin{bmatrix} \frac{1}{L_d(t)} & 0 \\ 0 & \frac{1}{L_q(t)} \end{bmatrix}}_{B(t)} \begin{bmatrix} u_d(t) \\ u_q(t) \end{bmatrix} - \begin{bmatrix} 0 \\ \frac{\Psi_p p\omega_r(t)}{L_q(t)} \end{bmatrix}. \tag{5}$$

At high flux densities, as occur when high torque is required, saturation effects occur in the iron of the PMSM, which means that the inductances must be considered as functions of the currents i_d and i_q:

$$L_d = f_{L_d}(i_d, i_q) \;;\; L_q = f_{L_q}(i_d, i_q). \tag{6}$$

The course of the inductances in dependence of the currents is presented in Figs. 2 and 3. The components $\frac{dL_d}{dt}$ and $\frac{dL_q}{dt}$ are neglected in order to simplify the model to be used in the EKF. It has to be noted, that the EKF is able to manage such kind of simplifications and can be included in its process noise. The torque is calculated in (7) and consists of the main torque as well as the reluctance torque due to the different inductances L_d and L_q.

$$T(t) = \frac{3}{2}p\Big\{ i_q(t)\Psi_p + (L_d(t) - L_q(t))i_d(t)i_q(t) \Big\}. \tag{7}$$

3. Calculation of two univariate polynomials

The dependence of the saturable inductances L_d and L_q is often more pronounced in the direction of one current component, i_d or i_q. As given in [25], due to the control with a negative current component for i_d, the dependence of the inductances for the i_q current is assumed to be higher. Therefore, the calculation of the univariate polynomial shall be considered as sufficient. For this reason, observing Figs. 2 and 3, it is possible to notice that the variation of L_d and L_q with respect to i_d is very small. The idea is to consider a univariate polynomial approximation for both. In other words, the proposal is to obtain

$$L_d \approx f_{L_d}(i_q) \;;\; L_q \approx f_{L_q}(i_q). \tag{8}$$

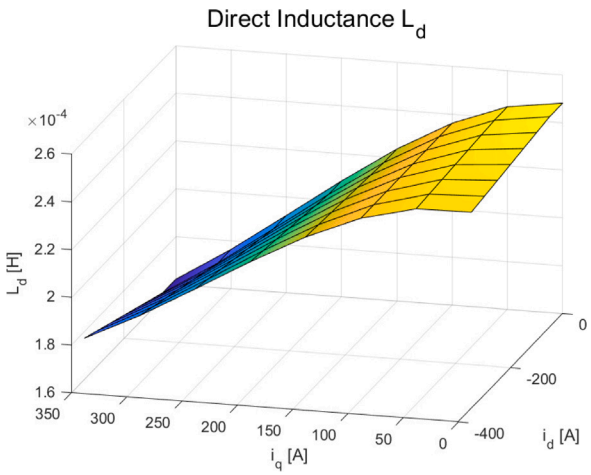

Fig. 2. Course of the characteristic field for L_d.

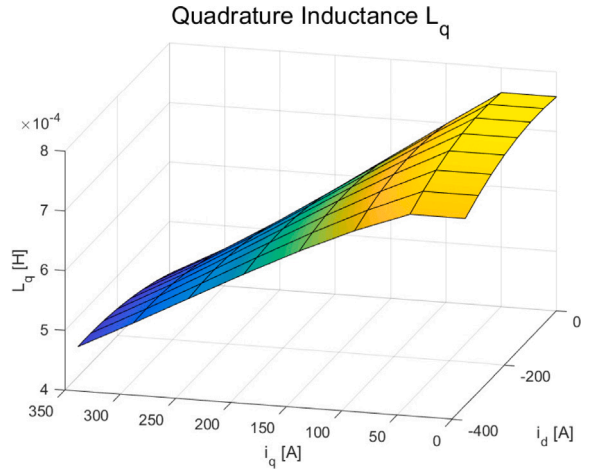

Fig. 3. Course of the characteristic field for L_q.

The general form of a univariate polynomial is given by:

$$f := n \to \sum_{i=0}^{n} a_i x^i, \tag{9}$$

in which the coefficients $a_0, a_1, \ldots, a_n \in \mathbb{R}$. For $a_n \neq 0$, $n \in \mathbb{N}$ define the grade of the polynomial. More details can be found in [48]. To calculate the univariate polynomial for the current dependent inductance, the coefficients in (10) with $\Theta_d(i_d, i_q)$ and $\Theta_q(i_d, i_q)$ have to be calculated. To distinguish between d and q current dependence, the two general univariate polynomials have to be calculated in both current directions for the coefficients $\Theta_d(i_d, i_q) = \Theta_d$ and $\Theta_q(i_d, i_q) = \Theta_q$.

$$\Theta = \begin{bmatrix} \Theta_d \\ \Theta_q \end{bmatrix} = \begin{bmatrix} X_d^T X_d \\ X_q^T X_q \end{bmatrix}^{-1} \begin{bmatrix} X_d^T L_d(d) \\ X_q^T L_q(q) \end{bmatrix}, \tag{10}$$

where $L_q(d)$ and $L_q(q)$ are the quadrature inductances in dependence of the currents i_d and i_q, which are taken out from the diagram. X_d and X_q are calculated with the current vectors I_d and I_q:

$$\mathbf{I_d} = -\begin{bmatrix} 350 & 300 & 250 & 200 & 150 & 100 & 50 & 0 \end{bmatrix} \tag{11}$$

and

$$\mathbf{I_q} = \begin{bmatrix} 0 & 50 & 100 & 150 & 200 & 250 & 300 & 350 \end{bmatrix}. \tag{12}$$

Each current vector, the direct and quadrature, includes *eight* elements. Matrix X_d is calculated as follows:

$$X_d = \begin{bmatrix} \mathbf{I_d^{3T}} & \mathbf{I_d^{2T}} & \mathbf{I}_{8\times1}^T \end{bmatrix}, \tag{13}$$

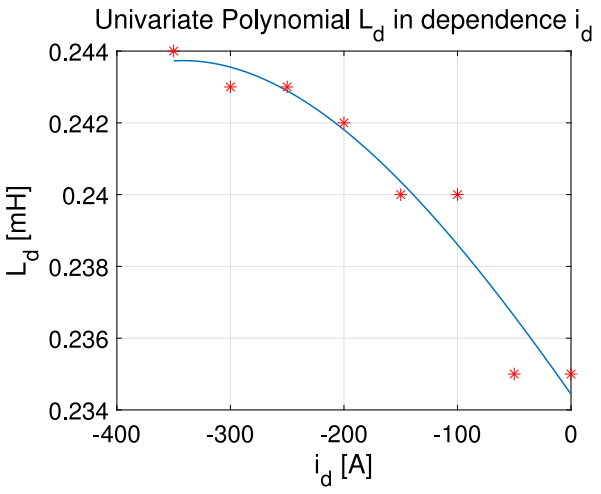

Fig. 4. Calculated univariate polynomial L_d in dependence of i_d.

in which $\mathbf{I}_{8\times1}$ represents the row of elements with values equaling one and matrix X_q is calculated as follows:

$$X_q = \begin{bmatrix} \mathbf{I_q^{3T}} & \mathbf{I_q^{2T}} & \mathbf{I}_{8\times1}^T \end{bmatrix}. \tag{14}$$

For the calculation of the univariate polynomials of the inductances L_d and L_q, expression (9) is taken into account with $n = 3$ in our case, which is reflected in (13) and in (14). The choice of the order of the polynomial is done considering index $R_{adj}(n, \Theta)^2$. It is to recall that $R_{adj}(n, \Theta)^2$ represents a statistical measure related to the proportion of the variance for a dependent variable that is explained by an independent variable or variables in a regression model. In the proposed application it is chosen $n^\star$ as the smallest n argument of the set of the calculated $R_{adj}(n, \Theta)^2$ minima, which is the grade of polynomial, calculated as follows:

$$S_{(n,\Theta)} = \left\{ (n, \Theta) : \arg\min_n \left(\arg\max_{\Theta} R_{adj}(n, \Theta)^2 \right) \right\} \tag{15}$$

in which $S_{(n,\Theta)}$ is the set of the arguments of minima of the non-convex optimization problem and

$$(n^\star, \Theta^\star) = \min_n S_{(n,\Theta)}, \tag{16}$$

with $\Theta^\star$ the values of the general parameters Θ as indicated in (10) corresponding to $n^\star$. The idea in (16) is to select from the set of the minima of $R_{adj}(n, \Theta)^2$ the minimum with the argument $(n^\star, \Theta^\star)$. In our case $n^\star = 3$ and $\Theta^\star$ which consists of a vector with eight components in accordance with (10): four components for $\Theta_d^\star$ and four components for $\Theta_q^\star$. The choice of $n^\star$, as the minimum order of the polynomial, reflects the necessity to obtain a compromise between approximation and calculation load. It is to notice that $\max_\Theta R_{adj}(n, \Theta)^2 = \min_\Theta SSE$, where SSE is the sum of squared errors, more details about this aspect can be found in the discussion and analysis Section 7. From Figs. 4 and 5 it is possible to see how L_d depends basically on i_q and thus it is possible to write as follows:

$$L_d(i_q) = \Theta_d(1) i_q(t)^3 + \Theta_d(2) i_q(t)^2 + \Theta_d(3) i_q(t) + \Theta_d(4). \tag{17}$$

The same calculations have to be done for the coefficients of the current dependent inductance L_q, to get the following equation. In the same way from Figs. 6 and 7 inductance L_q also depends basically on current i_q and thus it is possible to write as follows:

$$L_q(i_q) = \Theta_q(1) i_q(t)^3 + \Theta_q(2) i_q(t)^2 + \Theta_q(3) i_q(t) + \Theta_q(4). \tag{18}$$

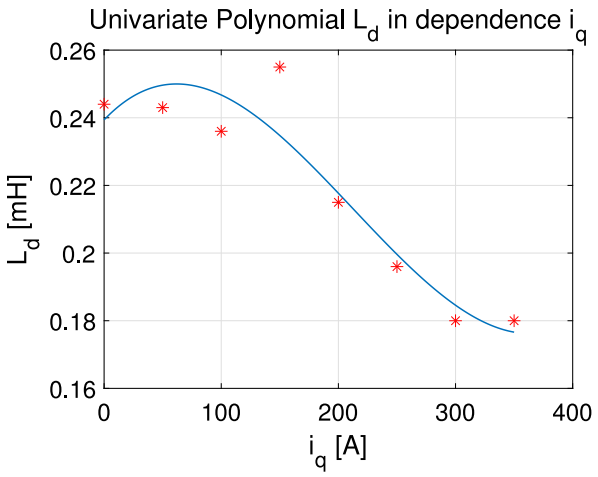

Fig. 5. Calculated univariate polynomial L_d in dependence of i_q.

4. A geometric approach for a noninteraction controller

In (5) it can be seen, that the d-portion influences the q-axis of the equation, just as the q-portion influences the d-axis in the opposite direction. This effect is called the cross coupling effect and comes from the fact, that the d-current component leads to a pre saturation in the q-axis as well as the q-current component is leading to pre saturation in the d-axis. The advantages of decoupling in PMSM are known. The geometric approach offers effective tools to realize a noninteracting control strategy, starting from the following Definition stated for a linear system of five maps (A, B, C, E), in which A is the transition, B the input, C the measured and E the output matrices respectively, see [49], page 298.

Definition 1 (*Noninteracting controller*)**.** A control law is said to be noninteracting with respect to partition $(e_1, \dots, e_k)$ of output e if there exists a corresponding partition $(r_1, \dots, r_k)$ of the reference input r such that, starting at the zero state, by acting on a single input r_i (with all the other inputs, d included, identically zero) only the corresponding output e_i is changed, while the others remain identically zero.

The existence of a noninteracting controller for a given output partition is strictly related to the structure of the system. Noninteraction is clearly related to the concept of constrained controllability. In fact, let

$$\mathcal{E}_i = \bigcap_{j \neq i}^{N} \ker E_i \quad (i = 1, \dots, k) \quad with \quad k \in \mathbb{N}. \tag{19}$$

It is clear that the reachable set on $\mathcal{E}_i$, i.e.

$$\mathcal{R}_{\mathcal{E}_i} = \mathcal{V}_i \cap \operatorname{min}\mathcal{S}(A, \mathcal{E}_i, \mathcal{B}) \quad (i = 1, \dots, k) \tag{20}$$

with

$$\mathcal{V}_i = \operatorname{max}\mathcal{V}(A, B, \mathcal{E}_i) \quad (i = 1, \dots, k) \tag{21}$$

is the maximal subspace on which, starting at the origin, state trajectories can be obtained that affect only output e_i, without influencing the other outputs, which remain identically zero. Subspace $\mathcal{V}_i$ is "the maximal" $(A, \mathcal{B})$ controlled invariant subspace contained in $\mathcal{E}_i$ and subspace $\mathcal{S}_i$ is called "the minimal" $(A, \mathcal{E}_i)$ conditioned invariant subspace containing $\mathcal{B}$. Therefore, conditions

$$E_i \mathcal{R}_{\mathcal{E}_i} = \operatorname{im} E_i \quad (i = 1, \dots, k) \tag{22}$$

are necessary and sufficient conditions to perform a complete noninteracting control. They clearly depend on the system structure, hence are necessary whatever the type of controller used (for instance a nonlinear one). Necessary and sufficient conditions for the existence of a noninteracting control are stated in Theorem 5.5.1 of pages 299–300, see [49]. It is also known, see [49], that if $\operatorname{min}S(A, \mathcal{E}_i, \mathcal{B}) = \mathcal{B}$ a linear system can be decoupled if and only if exists a matrix F:

$$(A + BF)\mathcal{V}_i \subseteq \mathcal{V}_i \qquad (i = 1, \dots, k). \tag{23}$$

Still in [49], it was shown that in case $(A, \mathcal{B})$ is controllable it is possible to place all external eigenvalues with respect to any $\mathcal{V}_i$, see Property 4.1.16 page 214. The constrained reachable set on $\mathcal{E}_i$ is $\mathcal{R}_{\mathcal{E}_i} = \operatorname{min}\mathcal{I}((A + BF), \operatorname{im} B \cap \mathcal{V}_i)$, see Theorem 4.1.6 of pages 210–211 in [49], and thus it follows $\operatorname{im} B \cap \mathcal{V}_i \neq 0$. In our specific case $k = 2$ and to realize the noninteraction, the following case with just two subspaces can be considered:

$$\mathcal{V}_1 = \operatorname{im} \begin{bmatrix} 1 \\ 0 \end{bmatrix} \tag{24}$$

and

$$\mathcal{V}_2 = \operatorname{im} \begin{bmatrix} 0 \\ 1 \end{bmatrix}. \tag{25}$$

It can be shown that

$$\mathcal{V}_1 = \operatorname{max}\mathcal{V}(A, B, \mathcal{E}_1) \cap \operatorname{min}\mathcal{S}(A, \mathcal{E}_1, \mathcal{B}) = \operatorname{im} \begin{bmatrix} 1 \\ 0 \end{bmatrix} \tag{26}$$

and also

$$\mathcal{V}_2 = \operatorname{max}\mathcal{V}(A, B, \mathcal{E}_2) \cap \operatorname{min}\mathcal{S}(A, \mathcal{E}_2, \mathcal{B}) = \operatorname{im} \begin{bmatrix} 0 \\ 1 \end{bmatrix}, \tag{27}$$

and that

$$\operatorname{im} B(t) \cap \mathcal{V}_i \neq 0 \quad (i = 1, 2). \tag{28}$$

Since the angular velocity variable is not included as a state of the system, the time-varying system defined in (5) is a time-varying one and on the light of the previous considerations, the following results are formally stated.

Proposition 1. *Given the time-varying system defined in (5), in accordance with condition of (28), no-left invertible system, a matrix $F(\omega_r)$ can be designed in order to satisfy condition (23), which satisfies also the stability problem.*

Proof. It is straightforward to show that the system is controllable because $\operatorname{rank} B(t) = n \; \forall \; t$, where n is the number of states and in which $B(t)$ is defined in (5). In the same way

$$\operatorname{im} B(t) \cap \mathcal{V}_i \neq 0 \tag{29}$$

is guaranteed $\forall i$ and $\forall t$. Condition (23) can be explicitly rewritten as follows:

$$\begin{bmatrix} \frac{-R_s}{L_d(t)} & \frac{L_q(t) p \omega_r(t)}{L_d(t)} \\ -\frac{L_d(t) p \omega_r(t)}{L_q(t)} & \frac{-R_s}{L_q(t)} \end{bmatrix} + \begin{bmatrix} \frac{1}{L_d(t)} & 0 \\ 0 & \frac{1}{L_q(t)} \end{bmatrix} F(\omega_r(t)) = \begin{bmatrix} \lambda & 0 \\ 0 & \lambda \end{bmatrix}. \tag{30}$$

Matrix $F(\omega_r)$ can be calculated as follows:

$$\begin{bmatrix} \frac{F_{11} - R_s}{L_d(t)} & \frac{F_{12} + L_q(t) p \omega_r(t)}{L_d(t)} \\ \frac{F_{21} - L_d(t) p \omega_r(t)}{L_q(t)} & \frac{F_{22} - R_s}{L_q(t)} \end{bmatrix} = \begin{bmatrix} \lambda & 0 \\ 0 & \lambda \end{bmatrix}, \tag{31}$$

which implies:

$$\begin{aligned} F_{11} &= R_s + L_d(t)\lambda; & F_{12} &= -L_q(t) p \omega_r(t) \\ F_{21} &= L_d(t) p \omega_r(t); & F_{22} &= R_s + L_q(t)\lambda. \end{aligned} \tag{32}$$

□

Remark 1. In (30) the two eigenvalues of the dynamics of the currents could be the same and this can be calculated by using matrix $F(\omega_r(t))$. Parameter λ represents the eigenvalues of the desired electrical system. For stability, λ must lie in the negative real plane. By adjusting the values of λ, we can obtain the desired dynamics of the electrical system of the synchronous motor.

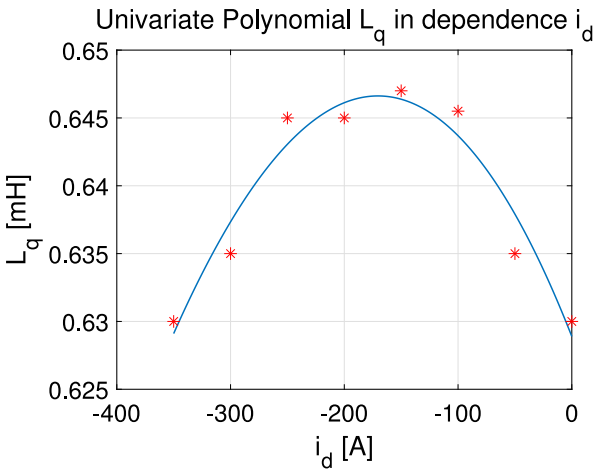

Fig. 6. Calculated univariate polynomial L_q in dependence of i_d.

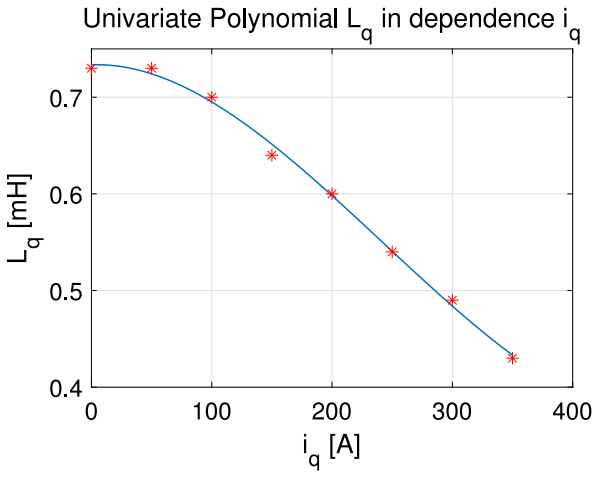

Fig. 7. Calculated univariate polynomial L_q in dependence of i_q.

The proof of Proposition 1 is a constructive one. The time-varying state–space decoupling controller, which is the key point of the proposed non-interacting control strategy, can be represented as shown in Fig. 1, as follows:

$$\begin{bmatrix}\tilde{u}_d(t)\\ \tilde{u}_q(t)\end{bmatrix} = \underbrace{\begin{bmatrix}R_s + L_d(t)\lambda & -L_q(t)p\omega_r(t)\\ L_d(t)p\omega_r(t) & R_s + L_q(t)\lambda\end{bmatrix}}_{F(\omega_r(t))}\begin{bmatrix}i_d(t)\\ i_q(t)\end{bmatrix}. \tag{33}$$

After the cancellation due to the time-varying state–space decoupling controller, and after the cancellation of term $\frac{\Psi_p p\omega_r(t)}{L_q(t)}$ using a u_{ff} feedforward action, see Fig. 1, as follows:

$$u_{ff}(t) = L_q(t)\frac{di_q(t)}{dt} + R_s i_q(t) + \Psi_p p\omega_r(t), \tag{34}$$

considering the system described in (1) and in (2), the following system is obtained:

$$\begin{bmatrix}\frac{di_d(t)}{dt}\\ \frac{di_q(t)}{dt}\end{bmatrix} = \underbrace{\begin{bmatrix}\lambda & 0\\ 0 & \lambda\end{bmatrix}}_{A_{dec}}\begin{bmatrix}i_d(t)\\ i_q(t)\end{bmatrix} + \begin{bmatrix}\frac{1}{L_d(t)} & 0\\ 0 & \frac{1}{L_q(t)}\end{bmatrix}\begin{bmatrix}v_d(t)\\ v_q(t)\end{bmatrix} \tag{35}$$

in which v_d and v_q are two supplementary inputs.

If the cancellation is not perfect, then, considering additive uncertainties $\hat{L}_d(t) = L_d(t) + \Delta_{L_d}$ and $\hat{L}_q(t) = L_q(t) + \Delta_{L_d}$, matrix A_{dec} becomes

$$\tilde{A}_{dec} = \begin{bmatrix}\lambda + \lambda(\Delta_{L_d}) & \Delta_d\\ \Delta_q & \lambda + \lambda(\Delta_{L_q})\end{bmatrix} \tag{36}$$

in which Δ_{L_d}, Δ_{L_q}, Δ_d and Δ_q represent the time-varying cancellation errors due to the non-perfect knowledge of the system. The system represented in (35) becomes

$$\begin{bmatrix}\frac{di_d(t)}{dt}\\ \frac{di_q(t)}{dt}\end{bmatrix} = \underbrace{\begin{bmatrix}\lambda + \lambda(\Delta_{L_d}) & \Delta_d\\ \Delta_q & \lambda + \lambda(\Delta_{L_q})\end{bmatrix}}_{\tilde{A}_{dec}(t)}\begin{bmatrix}i_d(t)\\ i_q(t)\end{bmatrix} + \begin{bmatrix}\frac{1}{L_d(t)} & 0\\ 0 & \frac{1}{L_q(t)}\end{bmatrix}\begin{bmatrix}v_d(t)\\ v_q(t)\end{bmatrix} - \begin{bmatrix}0\\ \Delta_{ff}\end{bmatrix}. \tag{37}$$

As explained, parameter Δ_{L_d}, Δ_{L_q}, Δ_d, Δ_q and Δ_{ff} represent the time-varying cancellation errors due to the non perfect knowledge of the system. In particular, term Δ_{ff} represents the time-varying cancellation error due to the uncertainties of the feedforward action u_{ff} defined in (34). These elements will be stochastically included in the process noise of the two corresponding EKFs.

Remark 2. Considering that ω_r is not a state of the system, matrix $\tilde{A}_{dec}(t)$ is basically a time-varying matrix and in accordance with [50] page 114, then the asymptotical stability of the system represented by the time-varying matrix $\tilde{A}_{dec}(t)$ is given by the sufficient condition that the real part of the eigenvalues of $\tilde{A}^T_{dec}(t) + \tilde{A}_{dec}(t)$ results to be strictly negative. This implies to find a λ such that $2\lambda + 2\Delta_{L_d}\lambda < 0$ and $(\lambda + \lambda(\Delta_{L_d}))(\lambda + \lambda(\Delta_{L_q})) - (\Delta_d + \Delta_q)^2 > 0$. These two conditions represents the Sylvester criterion for a matrix 2×2 to have negative eigenvalues. It is straightforward to show that choosing λ sufficiently large and negative, both conditions are satisfied.

4.1. Outer loop control using two PI controllers for the time-varying system

To robustify the control strategy, a PI controller is used as shown in Fig. 1. Considering the state representation of the PI controller included in the outer loop it is straightforward to show, in case of perfect cancellation of the element $\frac{\Psi_p p\omega_r(t)}{L_q(t)}$, it can be written as Eq. (38) in Box I where matrix $\tilde{A}_{PI}(t)$ is also a time-varying matrix and in accordance with [50] and above mentioned Sylvester theorem, the four Sylvester conditions on the determinants of the minors of the left corner can be easily satisfied by the four parameters of the two PI controllers: K_{pd}, K_{pq}, K_{Id} and K_{Iq}. States X_{Id} and X_{Iq} are the augmented states with which the two integral actions are described what can be seen in detail together with the proportional actions, in accordance with Fig. 1, as follows:

$$v_d(t) = K_{pd}(i_{dd}(t) - i_d(t)) + K_{Id}\underbrace{\int_0^t (i_{dd}(\tau) - i_d(\tau))d\tau}_{X_{Id}(t)} \tag{39}$$

and

$$v_q(t) = K_{pq}(i_{qd}(t) - i_q(t)) + K_{Iq}\underbrace{\int_0^t (i_{qd}(\tau) - i_q(\tau))d\tau}_{X_{Iq}(t)}. \tag{40}$$

Considering that, in accordance with Remark 2, it is possible to choose eigenvalues which guarantee the asymptotical stability of the controlled system and because of the dq transformation, i_d and i_q are constant after the transient and being i_{dd} and i_{qd} also constant after the transient, then $\frac{dX_{Id}(t)}{dt} = 0$ and $\frac{dX_{Iq}(t)}{dt} = 0$, which implies $i_d = i_{dd}$ and $i_q = i_{qd}$ after the transient.

$$\begin{bmatrix} \frac{di_d(t)}{dt} \\ \frac{di_q(t)}{dt} \\ \frac{dX_{Id}(t)}{dt} \\ \frac{dX_{Iq}(t)}{dt} \end{bmatrix} = \underbrace{\begin{bmatrix} \lambda + \lambda(\Delta_{L_d}) - \frac{K_{pd}}{L_d(t)} & \Delta_d & \frac{K_{Id}}{L_d(t)} & 0 \\ \Delta_q & \lambda + \lambda(\Delta_{L_q}) - \frac{K_{pq}}{L_q(t)} & 0 & \frac{K_{Iq}}{L_q(t)} \\ -1 & 0 & 0 & 0 \\ 0 & -1 & 0 & 0 \end{bmatrix}}_{\tilde{A}_{PI}(t)} \begin{bmatrix} i_d(t) \\ i_q(t) \\ X_{Id}(t) \\ X_{Iq}(t) \end{bmatrix} + \begin{bmatrix} \frac{K_{pd}}{L_d(t)} & 0 \\ 0 & \frac{K_{pq}}{L_q(t)} \\ 1 & 0 \\ 0 & 1 \end{bmatrix} \begin{bmatrix} i_{dd}(t) \\ i_{qd}(t) \end{bmatrix} - \begin{bmatrix} 0 \\ \Delta_{ff} \\ 0 \\ 0 \end{bmatrix} \tag{38}$$

Box I.

5. An EKF for inductance estimation for and within noninteracting control

In the EKF, the saturated inductance is estimated and fed back to the input of the noninteraction controller to determine the decoupling. The decoupling by means of a noninteraction control leads to the fact that the matrices of the EKF for the estimation of the saturated inductance, and thus the accompanying computational effort, can be reduced significantly. In the meantime, the quality of observability increases with the reduction of the variable to be estimated in each EKF. Despite the presence of the uncertainties Δ due to the non-perfect cancellation, the EKF, thanks to its stochastic structural nature, can estimate the inductance in an adequate way. Concerning some background of the EKF, the reader is addressed to Appendix. Moreover, in Section 7 the analysis and the discussion related to the observability of the decoupled system for the estimation of the inductances is considered. It is pointed out how additional white noise is artificially introduced to improve the observability of the system to be observed, see [35]. In the Appendix, the speed of the convergence of the proposed EKFs through the analysis of the a posteriori variance of the estimated variables is discussed.

5.1. EKF for inductance estimation

By discretizing the current equations in (1) and (2) and taking the decoupling calculations into account, we get the following discretized Eqs. (41) and (42):

$$\tilde{i}_d \approx \frac{i_d(k+1) - i_d(k)}{T_s} = \left(i_d(k)\lambda + \frac{v_d(k)}{L_d(k)} \right). \tag{41}$$

$$\tilde{i}_q \approx \frac{i_q(k+1) - i_q(k)}{T_s} = \left(i_q(k)\lambda + \frac{v_q(k)}{L_q(k)} \right). \tag{42}$$

Again, decoupling reduces the size of the equations. The factor λ must be taken into account.

While comparing (4) with (5), it is possible to see that the independence of the saturation effect in L_d strongly depends on the current i_q. The dynamics of L_d and L_q for the a priori estimation in both EKFs, EKFd and EKFq, see Fig. 1, are calculated as follows from (17) and (18):

$$\frac{L_d(k+1) - L_d(k)}{T_s} = 3\Theta_d(1) i_d(k)^2 \tilde{i}_d + 2\Theta_d(2) i_d(k) \tilde{i}_d + \Theta_d(3) \tilde{i}_d \tag{43}$$

and

$$\frac{L_q(k+1) - L_q(k)}{T_s} = 3\Theta_q(1) i_q(k)^2 \tilde{i}_q + 2\Theta_q(2) i_q(k) \tilde{i}_q + \Theta_q(3) \tilde{i}_q, \tag{44}$$

where $\tilde{i}_d$ and $\tilde{i}_q$ are defined in accordance with Euler discretization in (41) and (42). The discretized nonlinear system equations for i_d and L_d in (45) as well as the discretized nonlinear system equations for i_q and L_q in (46) are taken for the estimation of the a priori states $\hat{x}^-$ in the EKF in the prediction step as Eqs. (45) and (46) in Box II with $\tilde{i}_d$ and $\tilde{i}_q$ as derivatives (41) and (42) for the currents i_d and i_q. The values $\hat{i}_d$, $\hat{i}_q$, $\hat{L}_d$ and $\hat{L}_q$ are estimated at the previous step, see Appendix.

For the estimation of the a priori states $\hat{x}^-$ in the prediction step the EKF uses the a posteriori estimation $\hat{x}$ of the last iteration. The electrical model is described by nonlinear system equations, that makes it necessary for the estimation process of the EKF approach to derive the Jacobian matrices of the $d-$ and $q-$ components of the electrical systems after their decoupling:

$$J_d(k+1) = \begin{bmatrix} \frac{\partial i_d(k+1)}{\partial i_d(k)} & \frac{\partial i_d(k+1)}{\partial L_d(k)} \\ \frac{\partial L_d(k+1)}{\partial i_d(k)} & \frac{\partial L_d(k+1)}{\partial L_d(k)} \end{bmatrix}. \tag{47}$$

$$J_q(k+1) = \begin{bmatrix} \frac{\partial i_q(k+1)}{\partial i_q(k)} & \frac{\partial i_q(k+1)}{\partial L_q(k)} \\ \frac{\partial L_q(k+1)}{\partial i_q(k)} & \frac{\partial L_q(k+1)}{\partial L_q(k)} \end{bmatrix}. \tag{48}$$

After calculating the Jacobian matrix by using the estimation results of the last iteration, we get the following 2×2 matrices for the $d-$ and $q-$ components of the electrical systems after their decoupling:

$$J_d(k+1) = \begin{bmatrix} 1 + T_s\lambda & -T_s \frac{v_d(k)}{\hat{L}_d(k)^2} \\ J_{d_{21}} & J_{d_{22}} \end{bmatrix}. \tag{49}$$

$$J_q(k+1) = \begin{bmatrix} 1 + T_s\lambda & -T_s \frac{v_q(k)}{\hat{L}_q(k)^2} \\ J_{q_{21}} & J_{q_{22}} \end{bmatrix}. \tag{50}$$

The elements $J_{d_{21}}$, $J_{d_{22}}$ and the elements $J_{q_{21}}$, $J_{q_{22}}$ are reported in Appendix.

6. Measurements and results

Fig. 8 shows the Typhoon HIL system with which the control structure is validated. In emerging topics the prototyping phase represents an essential validation part of the project. For the validation of control concepts, the hardware in the loop (HIL) concept is being used more and more frequently. Here, the electronic control units to be tested are not directly integrated into the real system, but into a test bench with a mathematical system simulation. By means of an appropriate electronic interface, the control unit is connected to the HIL platform so that, from its point of view, there is no difference between the test bench and the later controlled system [51]. The Typhoon HIL402 environment allows the simulation of a traction inverter as well as a PMSM. The advantage of using the HIL system is that the stored saturation characteristics of the inductance of the used PMSM can be easily compared with the values estimated by the EKF. The C-code generated in Simulink's embedded coder can now be implemented and tested directly in a real time environment. The following measurements and results were taken with HIL Scada, the HIL testbed of Typhoon. As it can be seen in Fig. 1, the estimated inductances L_d and L_q are directly given into the noninteracting control for decoupling action. Since the EKF regulates to the final estimated value only after a short settling process after starting the control, the KF used for L_d and L_q are switched on one after the other in order to avoid mutual oscillation. The switching on happens in less than $1s$. During that time the noninteracting controller sees the nominal value of the inductance.

The torque is presented within Fig. 9 and as already discussed, because of the introduction of artificial white noise in the measured current 'to improve the observability' of the decoupled system, the noise is reflected also in the torque control, see Section 7. The beneficial effect of adding white noise in the measured current is nevertheless visible in the speed of convergence of EKF. In fact, from Figs. 14 and 15 a very short time of convergence of the variances of the estimated variables is visible thanks to the increased level of the variability

$$\hat{x}_d^-(k+1) = \begin{bmatrix} \hat{i}_d^-(k+1) \\ \hat{L}_d^-(k+1) \end{bmatrix} = \begin{bmatrix} T_s\left(\hat{i}_d(k)\lambda + \frac{v_d(k)}{\hat{L}_d(k)}\right) + \hat{i}_d(k) \\ T_s\left(3\Theta_d(1)\hat{i}_d(k)^2\tilde{i}_d + 2\Theta_d(2)\hat{i}_d(k)\tilde{i}_d + \Theta_d(3)\tilde{i}_d\right) + \hat{L}_d(k) \end{bmatrix} \tag{45}$$

and

$$\hat{x}_q^-(k+1) = \begin{bmatrix} \hat{i}_q^-(k+1) \\ \hat{L}_q^-(k+1) \end{bmatrix} = \begin{bmatrix} T_s\left(\hat{i}_q(k)\lambda + \frac{v_q(k)}{\hat{L}_q(k)}\right) + \hat{i}_q(k) \\ T_s\left(3\Theta_q(1)\hat{i}_q(k)^2\tilde{i}_q + 2\Theta_q(2)\hat{i}_q(k)\tilde{i}_q + \Theta_q(3)\tilde{i}_q\right) + \hat{L}_q(k) \end{bmatrix} \tag{46}$$

Box II.

of the measured current, see Section 7. The proposed torque control strategy shows promising results in terms of reduction of its oscillations, bias between desired and obtained torque and disturbances, and the proposed control strategy maintains, at the same time, ripples inside the technical limits in the obtained torque. For validation, the torque is increased up to 150 N m. The torque ripple is based on the geometrical characteristics of the electric machine. Contributions like [52,53] show that a reduction of the torque ripple to 9% is possible if certain measures are taken into account in the geometrical design of the motor. As already explained, the torque ripple is related to structural geometrical characteristics of the machine and cannot be reduced significantly below these values. The torque ripple in Fig. 9 is 12% which illustrates that the control strategy used keeps the torque ripple at a consistently low level. Since the currents i_d and i_q are measured and given to the KF, the course of the respective estimated current value (shown here in red) follows that of the actual value. As the required torque is increased in portions, the current i_q in the PMSM increases, as it is shown in Fig. 10, while at the same time current i_d decreases, as it is shown in Fig. 11. The inductance deviates more and more from its nominal value as a result of the increase in flux density. Magnetic saturation results in a nonlinear relationship between magnetic field strength and flux density and a reduction in the effective inductance due to the saturated iron of the stator. Figs. 12 and 13 show the inductances L_d and L_q in blue. These actual inductances were measured and recorded on the component and machine test bench for electrical machines prior to the investigations with KF. The course of the estimated inductance values L_d and L_q by EKFs are shown in red. The estimation provides reliable values over the entire torque range. However, it can be clearly seen that for both L_d and L_q, a clear agreement between the estimated and nominal values occurs from a higher torque of 70 N m for L_q and 150 N m for the inductance L_d. The improvement of the estimation with the increase of torque and thus the increase of the currents i_d and i_q is due to the very small inductance values which have to be estimated. By increasing the current values, the calculation of the models stored in the KF become more accurate. In signal processing, when using microcontrollers, a very limited calculation load is always a suitable goal. An overview on the arithmetic operation requirements, as often is shown in literature, see [54,55], for the proposed EKF structure is shown in Table 1. This overview is related to the calculation load of each EKF. In this sense, the total calculation load is twice that shown in this table in which n, m and p represent the dimension of the state vector, the dimension of the input vector and the dimension of the measured output respectively. If the unique EKF is considered, then Table 2 is considered as overview of the calculation load. It is possible to see from Table 1 that thanks to the decoupled KF a very reduced calculation load is obtained as a result with respect to a non decoupled EKF as reported in Table 2. The Matlab code of the reduced EKFs is in Appendix.

7. Discussion and analysis

In this Section, measurements and results are discussed further together with future perspectives.

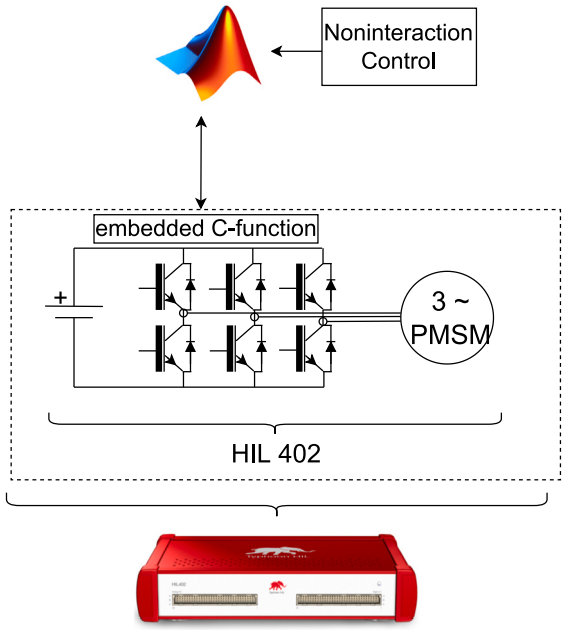

Fig. 8. Typhoon system for PMSM prototyping.

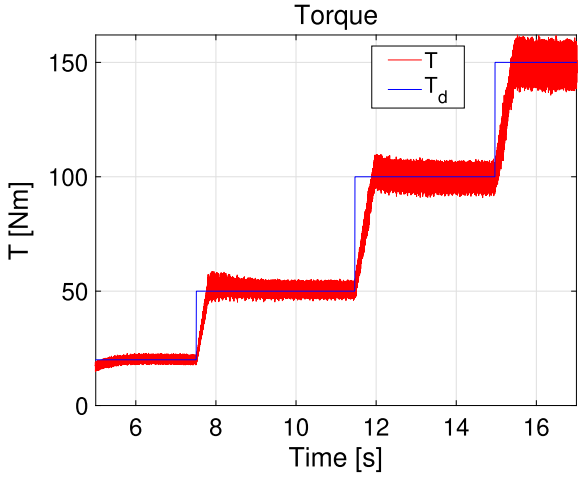

Fig. 9. Actual motor torque T and desired torque T_d. (For interpretation of the references to color in this figure legend, the reader is referred to the web version of this article.)

7.1. Contribution highlights

The main contribution is the estimation of nonlinear inductances in case of saturation. As it can be seen for example in [37], this

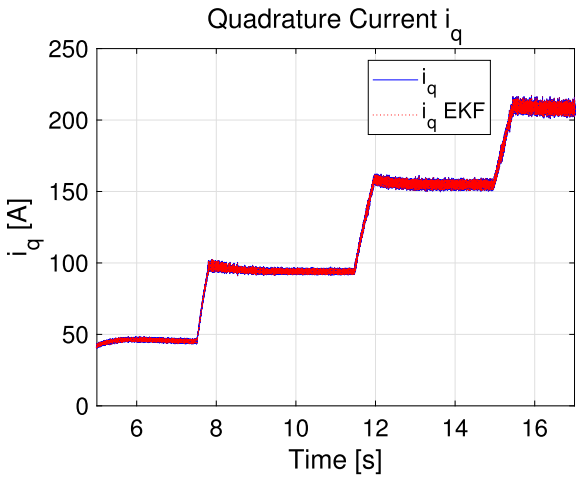

Fig. 10. Estimated and actual values for quadrature current i_q. (For interpretation of the references to color in this figure legend, the reader is referred to the web version of this article.)

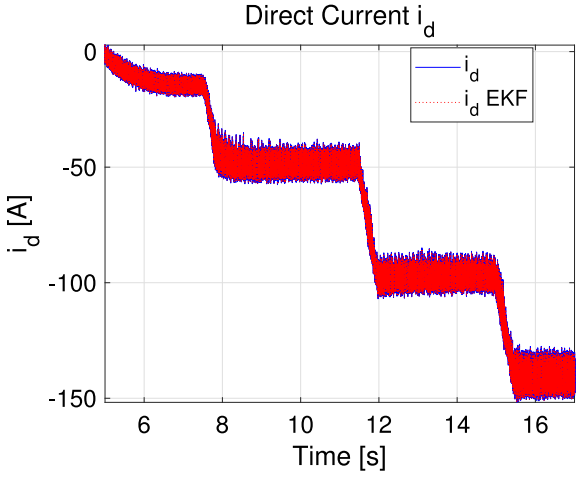

Fig. 11. Estimated and actual values for direct current i_d. (For interpretation of the references to color in this figure legend, the reader is referred to the web version of this article.)

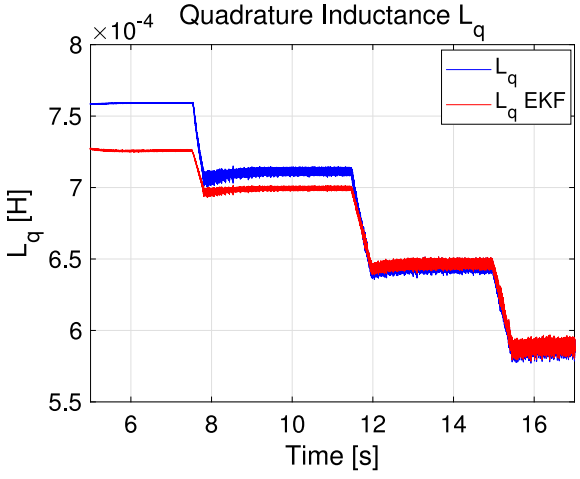

Fig. 12. Estimated and actual values for quadrature inductance L_q. (For interpretation of the references to color in this figure legend, the reader is referred to the web version of this article.)

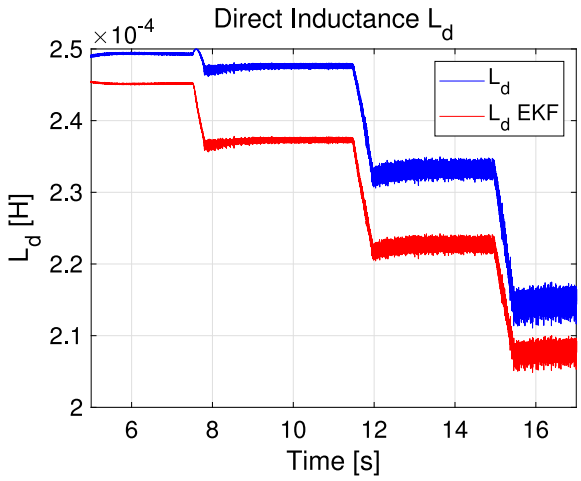

Fig. 13. Estimated and actual values for direct inductance L_d. (For interpretation of the references to color in this figure legend, the reader is referred to the web version of this article.)

Table 1
Overview of the arithmetic operation requirements for the proposed decoupled EKF structure.

	Number of multiplications (n = 2, m = 1, p = 1)	Number of additions (n = 2, m = 1, p = 1)
$\hat{\mathbf{x}}^-(k+1)$ Eq. (60)	n^2+nm (6)	n^2-n+nm (4)
$\mathbf{P}^-(k+1)$ Eq. (61)	$2n^3$(16)	$2n^3-n^2$ (12)
$\hat{\mathbf{x}}(k+1)$ Eq. (63)	$2nm+pm$ (5)	$2nm+pm$ (5)
$\mathbf{K}(k+1)$ Eq. (62)	$n^2m+2np^2+p^3$ (9)	$n^2m+2np^2+p^3-2np$ (12)
$\mathbf{P}(k+1)$ Eq. (65)	n^3+n^2p (12)	$n^3+n^2p-n^2$ (8)
Total	48	41

Table 2
Overview of the arithmetic operation requirements for the non decoupled EKF structure.

	Number of multiplications (n = 4, m = 2, p = 2)	Number of additions (n = 4, m = 2, p = 2)
$\hat{\mathbf{x}}^-(k+1)$ Eq. (60)	n^2+nm (20)	n^2-n+nm (20)
$\mathbf{P}^-(k+1)$ Eq. (61)	$2n^3$(128)	$2n^3-n^2$ (112)
$\hat{\mathbf{x}}(k+1)$ Eq. (63)	$2nm+pm$ (20)	$2nm+pm$ (20)
$\mathbf{K}(k+1)$ Eq. (62)	$n^2m+2np^2+p^3$ (72)	$n^2m+2np^2+p^3-2np$ (56)
$\mathbf{P}(k+1)$ Eq. (65)	n^3+n^2p (96)	$n^3+n^2p-n^2$ (80)
Total	144	288

kind of problem is still an open problem. The decoupling approach in combination with PI control for PMSM is a common control method for controlling an “almost” linear system. If the cancellation is perfect, then the linearization of the system can be guaranteed by decoupling. In a closed control loop, because of the non perfect estimation of the parameters a permanently maintained “almost” linear system is obtained. The big advantage of the decoupling controller here is that it leads to the use of the two decoupled EKF equations, which leads to much smaller matrices and thus to faster calculations due to lower

computational load, that is shown in Tables 1 and 2 of the contribution. This is particularly relevant in case of small sample times in the realization of the discrete controller. In the analyzed case the sample time equals 100 µs. Another big advantage of the two reduced order augmented decoupled EKFs is the increased observability quality, which is reflected in the tracking results. If we assume the structure of a centralized augmented EKF, it must be emphasized that the quality of observability decreases with the increasing number of parameters to be observed. To stay in the terminology of [33], it can be said that the quality of observability decreases or the system can even become unobservable, as shown for example in [56]. In contrast, if two smaller decoupled EKFs are used, this increases the quality in view of the local observability and therefore makes sense if the number of augmented states is increased. There are various ways to specify the measure of the quality of observability. These include the maximum eigenvalue, the trace or the determinant of the inverse observability Gramian. It is presented for example in [33,34] and in [46]. Possible candidate index for the measure of the quality of the local observability are the maximal eigenvalue, the trace or the determinant of the inverse observability Gramian. In [33,34] and in [46] it was shown how the quality of the observability and the quality of the local observability index can increase in case of separation of the observer structure, see [36]. If the approach for calculation of the EKF model is discussed, it can be clearly shown that a univariate polynomial in a decoupled EKF entails significantly less complexity compared to [35], where a bivariate polynomial is used to capture the current dependence in the d and q direction of the inductances. However, the great advantage in the usage of the univariate polynomial within the EKF model is that the univariate polynomial requires significantly fewer measured sampling points than in the case of using a bivariate polynomial. Especially if the electric motor is already permanently installed and coupled with the load to be turned, for example in a marine or train application, measuring the electrical inductances is only possible to a much limited extent.

7.2. Limitations

In general, there are two main types of PMSMs. The PMSMs with surface mounted magnets and the PMSM with buried magnets, also called interior PMSM. As the presented control is dealing with an MTPA in the outer control loop, the inductances L_d and L_q have to be unequal, which is only true for interior PMSM types. From the calculation of the desired currents i_{dd} and i_{qd} using this control structure, it follows that it is only valid for PMSMs with L_d not equal to L_q, which is a limitation for PMSMs with surface mounted magnets. The PMSM with buried magnets under test can be considered as low impedant due to their very small inductances. Since the low impedance of the machine makes it much more difficult to estimate the parameters, it can be concluded from this that the method presented is valid for a wide range of machines with interior magnets. The analysis also considers the validation method, which was carried out using a HIL test stand. HIL models are based on models in which calculation models are executed that include a simplification of the physical components. However, it must be noted that the underlying computational models are much more complex and accurate than they were a few years ago due to the development of much more powerful hardware components such as FPGAs, and the development of these models is still ongoing. This is not the only reason why HIL systems have made strong inroads into institutions and companies. The time and cost savings that come from successful use at an early stage of development make HIL validation one of the most important tools in the modern development of control algorithms. The HIL validation was able to show the quality of the estimation process of parameters and states in the saturation region of the PMSM and the use of the estimated parameters in an adaptive decoupling PI control. The objective of demonstrating parameter estimation for the non-linear operating range of the electrical machine can therefore be considered fulfilled.

7.3. Choice of the approximating univariate polynomials

The choice of the univariate polynomials was done according to the approach of the fitting problem. In the context under consideration, a fitting problem is used to obtain the inductances L_d and L_q as functions of the currents i_d and i_q. Univariate polynomials offer a lower computational effort and enable a smaller sampling time in the implementation of the microcontroller. A smaller sampling time allows the use of the feedforward Euler discretization method, which offers a structural advantage as it has an explicit structure in its model. The choice of the polynomials in (17) and in (18) is related to the indicator R-squared adjusted which is defined in the following way:

$$R_{adj}(n,\Theta)^2 = 1 - \left(\frac{m_o - 1}{m_o - p_c}\right)\frac{SSE}{SST}, \tag{51}$$

where m_o is the number of observations, n is the order of the polynomials and $p_c = n + 1$ is the number of regression coefficients. In which the following indicators are defined as follows. The sum of squared errors is $SSE = \sum_{i=1}^{m_o}(y_i - \hat{y}_i)^2$ and the total sum of squares is $SST = \sum_{i=1}^{m_o}(y_i - \bar{y})^2$, where y_i and $\bar{y}$ represent the measured points and their mean value. It is to recall that $R_{adj}(n,\Theta)^2$ is not a monotonic function with respect to variable n. Typically, a suitable choice of the order of the approximating polynomials is obtained considering one of the minimum of this indicator with respect to a sufficiently small order n of the polynomial. This is due in order to find a compromise between a reduced overfitting, enough precision of the approximation and a reduced order of the polynomial to obtain a reduction of the calculation load of the online algorithm. Considering the obtained value for $R_{adj}(n,\Theta)^2$ the minimum of it is found at $n = 3$ in our case. In particular, starting from $n = 0$, $R_{adj}(n,\Theta)^2$ decreases until $n = 3$ and at $n = 4$ it is already increased. One of the possible criteria is to choose the value of n in which the first minimum of $R_{adj}(n,\Theta)^2$ is obtained. A minimum for $R_{adj}(n,\Theta)^2$ reflects $SSE \approx SST$ which states the minimum of $SSR = \sum_{i=1}^{m}(\bar{y} - \hat{y}_i)^2$ which represents a statistical indicator.

7.4. Some concerns on the sampling time

The sample time T_s is a crucial parameter for the Kalman filter, as it determines how quickly the loop of calculations of the Kalman filter equations is repeated. This results in a certain advantage for the shortest possible sampling times, which no longer increases significantly after a certain point. The disadvantage of sample times that are too short, on the other hand, is that the computing power required by executing hardware components such as digital signal processors (DSPs) or field programmable gate arrays (FPGAs) increases inversely. For this reason, the sample time cannot be chosen to be arbitrarily small and must therefore be adjusted to an optimum. The Typhoon HIL hardware-in-the-loop test stand already provides important information about the adjustable sampling time. An FPGA works within the Typhoon HIL, which simulates the hardware of the inverter and electrical machine. As the simulation of the components is very computationally intensive, there is only limited computing power available to run the Kalman filter algorithms, despite the use of an FPGA module. In order to obtain a realistic image for determining the sampling time, the authors used a common DSP from Texas Instruments in [35], with the help of which a sampling time of $T_s = 10^{-4}$ s could be set. With this sampling time, it could be shown that the KF is able to estimate good and stable results and provide them to the adaptive control. The TI DSP F28335 used in [35] is a powerful DSP. Since it cannot always be guaranteed that this computing power is available for the execution of the calculations, the extent to which the sampling time can be increased by using a KF with backward Euler calculation was investigated by the authors in [36]. It could be shown that the required sample time T_s could be significantly increased to 10^{-4} s. In general it is known that backward Euler approximation offers more stability characteristics with respect to the forward Euler approximation, see [57].

7.5. Observability analysis

To highlight the advantage of the decoupling of the EKFs, some background related to the nonlinear observability concept is summarized together with its test in the proposed case. For more details on the nonlinear observability see [58]. At page 733 of [58] different concepts and corresponding definitions of observability are proposed: local observability, local weak observability, observability and weak observability. It is shown how, starting from the definitions of these concepts, the local observability implies the local weak observability which implies the weak observability and in the same way the local observability implies observability which implies the weak observability. Without going into detail of these definitions we can say that observability is a global concept and it might be necessary to travel a considerable distance or for a long time to distinguish between points in the domain of the definition of the system. In fact, a local observable system at a point results to be distinguishable for every open neighborhood of this point. A system is locally weakly observable at a point, if for every open neighborhood U of this point there exists a neighborhood V contained in U in which the state of the system is distinguishable. In other words, it is possible to instantaneously distinguish each point from its neighbors and a system is weak observable just if exists a neighborhood U such that its states are distinguishable at this point. The test which we have at disposition in the literature, see [58], is a test related to the local weak observability. This test is based on the use of Lie derivative structures. The concept is strictly connected with the concept of the distinguishability in finite time. A nonlinear System

$$\begin{cases} \dot{x}(t) = f(x,u) \\ y(t) = h(x) \end{cases} \tag{52}$$

is locally weak observable if

$$\mathrm{rank}(\mathbf{O}(\mathrm{x},\mathrm{u},\mathrm{t})) = \begin{bmatrix} \mathbf{O}_0 \\ \mathbf{O}_1 \\ \mathbf{O}_2 \\ \cdots \\ \mathbf{O}_{n-1} \end{bmatrix} = \mathrm{n}. \tag{53}$$

Please notice that condition (53) which states a sufficient condition can be rewritten as

$$\mathbf{O}(x,u,t) = \begin{bmatrix} \frac{\partial h}{\partial x^T} \\ \frac{\partial O_0 f}{\partial x^T} \\ \frac{\partial O_1 f}{\partial x^T} \\ \cdots \\ \frac{\partial O_{n-1} f}{\partial x^T} \end{bmatrix} = \begin{bmatrix} \frac{\partial h}{\partial x^T} \\ \frac{\partial L_f h}{\partial x^T} \\ \frac{\partial L_f^2 h}{\partial x^T} \\ \cdots \\ \frac{\partial L_f^{n-1} h}{\partial x^T} \end{bmatrix}. \tag{54}$$

Being the decoupled system to be observed representable for the "d-dynamics" in the following form:

$$\begin{cases} \frac{di_d(t)}{dt} = -\frac{R_s i_d(t)}{L_d(t)} + \frac{u_d(t)}{L_d(t)} \\ \frac{dL_d(i_q(t))}{dt} = \left(3\Theta_q(1) i_q(t)^2 + 2\Theta_q(2) i_q(t) + \Theta_q(3)\right) \tilde{i}_q, \end{cases} \tag{55}$$

where $\tilde{i}_q$ is the derivative of i_q.

When applying (53) and (54) it is possible to obtain the following matrix:

$$\mathbf{O}(i_d, L_d, u_d, t) = \begin{bmatrix} 1 & 0 \\ \star & -\frac{R_s i_d(t) + u_d(t)}{L_d(t)^2} \end{bmatrix}, \tag{56}$$

where $\star$ is not needed to be calculated because its expression does not influence the determinant. To conclude $det(\mathbf{O}(i_d, L_d, u_d, t)) \neq 0$ for

$$\frac{R_s i_d(t) - u_d(t)}{L_d(t)} \neq 0. \tag{57}$$

This is equivalent to

$$\frac{di_d(t)}{dt} \neq 0. \tag{58}$$

Similar consideration can be done for the decoupled "q-dynamics" to obtain the following condition for the local weak observability:

$$\frac{di_q(t)}{dt} \neq 0. \tag{59}$$

Remark 3. Condition (58) and (59) state the sufficient condition for the local weak observability to be guaranteed also after the transient. Therefore, a white noise is deliberately introduced in the measurements of i_d inside the EKF to guarantee the sufficient condition.

7.6. Future work and perspectives

The presented method for estimating saturated inductances using a decoupling EKF together with a univariate polynomial can be used in further control strategies. For example, the improvement of the behavior of a model predictive control (MPC) would have to be investigated, since the mapping of the model will represent a higher degree of accuracy than by using nominal parameters. Another possibility is the use of the estimation method in combination with a sliding mode control (SMC), which works very robustly against parameter uncertainties, but also possibly gains significant advantages by more accurate parameters in the dynamics. As it is shown in [59], the usage of a SMC together with an MTPA approach in the outer control loop is very effective. It would be very interesting, if it would be possible to reduce the calculation load by help of the use of two decoupled EKFs and univariate polynomials for the KF model together with the more computationally intensive SMC. In order to explain whether the control algorithm presented in this contribution can be used in addition to the control of PMSMs, it can be shown in the context of decoupling control that the field of application of this control is very broad and is widely used in a variety of areas. For example, [60] shows a distributed decoupling algorithm which is used in multi-agent systems with nonlinear uncertainties. Also in the context of decoupling control, recent contributions in [61,62] show that the method can even be adapted for estimating the state of charge (SOC) in energy-storing lithium-ion batteries. To further illustrate the wide range of applications of decoupling control, the recently published paper [63] presents another example in which multiple-input–multiple-output (MIMO) systems are controlled using a calibrated decoupling matrix. The various decoupling algorithms can often be extended by an estimation algorithm such as EKF.

8. Conclusion

The estimation of the parameters L_d and L_q is fundamental for the application of the strategy of controlling the maximum torque per ampere in order to achieve an exact optimality of the reference currents i_d and i_q. Determining an appropriate optimum control system is a fundamental issue for reducing mechanical vibrations and interference. In this paper a non-interacting controller for a permanent magnet synchronous machine was presented, with the estimation of the parameters L_d and L_q for an adaptive non-interacting $d-$ and q-axis controlled system.

These two inductances are estimated by two extended Kalman filters, which use a univariate polynomial as a model to describe the saturation effects of the machine under consideration. The Kalman filters are realized with the decoupled system to improve the observability of the inductance and despite the imperfect decoupling.

Starting from the existing literature, a viable control structure is proposed in which the stability of the control loop using a PI controller is also shown for the resulting time-varying system.

$$J_{d_{21}} = T_s\left(\Theta_d(3)\lambda + 2\Theta_d(2)\left(\hat{i}_d^-(k)\lambda + \frac{v_d(k)}{\hat{L}_d^-(k)}\right) + 6\Theta_d(1)\hat{i}_d^-(k)\left(\hat{i}_d^-(k)\lambda + \frac{v_d(k)}{\hat{L}_d^-(k)}\right) + 2\Theta_d(2)\hat{i}_d^-(k)\lambda + 3\Theta_d(1)\hat{i}_d^-(k)^2\lambda\right) \tag{66}$$

$$J_{d_{22}} = 1 - T_s\left(\frac{\Theta_d(3)v_d(k)}{\hat{L}_d^-(k)^2} + \frac{2\Theta_d(2)\hat{i}_d^-(k)v_d(k)}{\hat{L}_d^-(k)^2} + \frac{3\Theta_d(1)\hat{i}_d^-(k)^2 v_d(k)}{\hat{L}_d^-(k)^2}\right) \tag{67}$$

$$J_{q_{21}} = T_s\left(\Theta_q(3)\lambda + 2\Theta_q(2)\left(\hat{i}_q^-(k)\lambda + \frac{v_q(k)}{\hat{L}_q^-(k)}\right) + 6\Theta_q(1)\hat{i}_q^-(k)\left(\hat{i}_q^-(k)\lambda + \frac{v_q(k)}{\hat{L}_q^-(k)}\right) + 2\Theta_q(2)\hat{i}_q^-(k)\lambda + 3\Theta_q(1)\hat{i}_q^-(k)^2\lambda\right) \tag{68}$$

$$J_{q_{22}} = 1 - T_s\left(\frac{\Theta_q(3)v_q(k)}{\hat{L}_q^-(k)^2} + \frac{2\Theta_q(2)\hat{i}_q^-(k)v_q(k)}{\hat{L}_q^-(k)^2} + \frac{3\Theta_q(1)\hat{i}_q^-(k)^2 v_q(k)}{\hat{L}_q^-(k)^2}\right) \tag{69}$$

Box III.

The proposed torque control strategy shows promising results in terms of reduction of its oscillations, bias between desired and obtained torque and disturbances. Moreover, the proposed control strategy maintains, at the same time, ripples inside the technical limits in the obtained torque. The effectiveness of the proposed torque control method, with very limited calculation load, is validated using real data within a hardware in the loop system.

CRediT authorship contribution statement

Tanja Zwerger: Writing – review & editing, Writing – original draft, Visualization, Validation, Software, Resources, Project administration, Methodology, Investigation, Formal analysis, Data curation, Conceptualization. **Paolo Mercorelli:** Writing – review & editing, Writing – original draft, Visualization, Validation, Supervision, Software, Resources, Project administration, Methodology, Investigation, Funding acquisition, Formal analysis, Data curation, Conceptualization.

Declaration of competing interest

The authors declare that they have no known competing financial interests or personal relationships that could have appeared to influence the work reported in this paper.

Acknowledgment

We thank the anonymous reviewers for their careful reading of our manuscript and their many insightful comments and suggestions.

Appendix

In this Appendix, two aspects are recalled and discussed: the background of Kalman filter equations as well as the analysis of the convergence of EKF in dependence to the observability quality that was shown in Section 7.

A.1. Kalman filter background

As we can see in [64], the a priori estimation is as follows:

$$\hat{x}^-(k+1) = f(\hat{x}(k), u(k), w(k)), \quad k \in \mathbb{N}, \tag{60}$$

in which function $f(\hat{x}, u, w)$ represents the nonlinear field used as model of the system, which is calculated at the previous corrective step.

The a priori error covariance of the state prediction is written in the following form:

$$P^-(k+1) = J(k+1)P(k)J(k+1)^T + Q, \tag{61}$$

where J is the Jacobian matrix, P represents the a posteriori error covariance matrix at the previous corrective step k. Matrix Q represents the covariance matrix of the process noise which quantifies the model uncertainty. Smaller values of the trace in this matrix, indicate a high reliability of the model. The Kalman gain K is as follows:

$$K(k+1) = P^-(k+1)H^T(HP^-(k+1)H^T + R_w)^{-1}, \tag{62}$$

with R_w as the covariance matrix for the measurement noise. The matrix H defines the output Jacobian. The a posteriori estimation is as follows:

$$\hat{x}(k+1) = \hat{x}^-(k+1) + K(k+1)(z(k+1) - H\hat{x}^-(k+1)), \tag{63}$$

where

$$z_k(k+1) = x(k+1) + v(k+1) \tag{64}$$

represents the measured data in which vector signal v represents the measured white Gaussian noise. The a posteriori estimation of the error covariance is as follows:

$$P(k+1) = (I - K(k+1)H)P^-(k+1). \tag{65}$$

A.2. Kalman filter matlab code and its Jacobian

In this section the Matlab code of the Kalman filter related to the i_d and L_d dynamics is shown. The i_q and L_q dynamics have similar Matlab code structure and for sake of brevity is omitted. Code is available in listing 1.

The following elements which are defined in Eqs. (66), (67), (68) and (69) given in Box III represent the components of the Jacobian matrices in (49) and (50) of the $d-$ and $q-$ components of the electrical systems after their decoupling.

A.3. A posteriori covariance matrix: analysis and discussion

It is known that observability is a necessary condition for the convergence of the EKF. In case of an EKF, the local weak observability condition in (53) and (54) represents just a sufficient condition. In this sense, the condition of the observability which we have at disposition is too weak for any conclusion related to the convergence of EKF. Nevertheless, it is suitable to satisfy the sufficient condition of the local weak observability in order to improve the convergence of the filter. As discussed before, condition (59) states the sufficient condition for the local weak observability. A white noise is deliberately introduced in the measurements of i_d and i_q inside the EKF to guarantee the sufficient condition and to speed up the convergence of it. In fact, observing Figs. 14 and 15, it is possible to see that the a posteriori error variance of the EKF decreases rapidly during the transient. To conclude, from Figs. 14 and 15 a very short time of convergence of the a posteriori variances of the estimated variables is visible thanks to the increased level of the variability of the measured current, see Appendix.

Listing 1: Matlab code

```
function [idEst,LdEst,Pid,PLd]= fcn(vdIn,idMess,parameters,Thetadid,iq)
% Memory variables that persist between execution cycles
persistent: old_states old_covariance;
% Parameters
R=parameters(1); %stator resistance
Ld0=parameters(3); %initial inductance value
Ts=parameters(8); %sample time
lambda=parameters(9); %eigenvalues of the electrical system

% Initial conditions
if isempty(old_states)
    %           id  Ld
    old_states=[0;  Ld0];
end

if isempty(old_covariance)
    old_covariance=[1  0;
                    0  1]*1e1;
end

% Assign old values
id=old_states(1);
Ld=old_states(2);

% EKF Parameters
Rw=1e-2; %covariance matrix for the measurement noise.

Qx=[1e-2  0; %covariance matrix for the process noise.
    0     1e-8];


didt=id*lambda*Ts+id+Ts/Ld*vdIn;

estimated_states=[id*lambda*Ts+id+Ts/Ld*vdIn;
                Ts*(Thetadid(1)*3*id^2*didt+Thetadid(2)*2*id*didt+Thetadid(3)*didt)+Ld];

%calculation of Jacobian matrix

Jc1=Ts*(Thetadid(3)*(Ts*lambda+1)+2*Thetadid(2)*(id+Ts*id*lambda+(Ts*vdIn)/Ld)...
+6*Thetadid(1)*id*(id+Ts*id*lambda+(Ts*vdIn)/Ld)+2*Thetadid(2)*id*(Ts*lambda+1)...
+3*Thetadid(1)*id^2*(Ts*lambda+1));
Jc2=1-Ts*((Thetadid(3)*Ts*vdIn)/Ld^2+(2*Thetadid(2)*Ts*id*vdIn)/Ld^2...
+(3*Thetadid(1)*Ts*id^2*vdIn)/Ld^2);

Jacobian=[1+Ts*lambda           -Ts*vdIn/Ld^2; %id
             Jc1    Jc2];
% Output Jacobian: outputs = id. evaluated in a-priori estimation!

H=[1 0];

% A-priori Covariance
estimated_covariance=Jacobian*old_covariance*Jacobian'+Qx;

% Kalman Gain
kalman_gain=estimated_covariance*H'/(H*estimated_covariance*H'+Rw);
innovation=idMess-H*estimated_states;
corrected_states=estimated_states+kalman_gain*innovation;
corrected_covariance=(eye(2)-kalman_gain*H)*estimated_covariance;

% Save values for next cycle
old_covariance=corrected_covariance;
old_states=corrected_states;

% Block output
idEst=corrected_states(1);
LdEst=corrected_states(2);
Pid=corrected_covariance(4);
PLd=corrected_covariance(1);
```

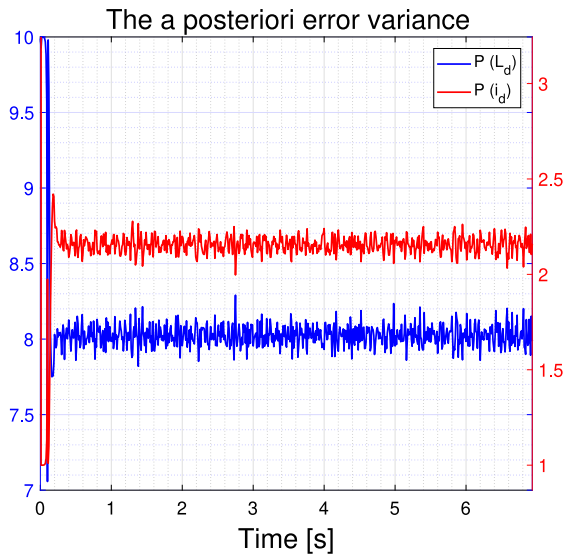

Fig. 14. A posteriori variance of i_d and L_d. (For interpretation of the references to color in this figure legend, the reader is referred to the web version of this article.)

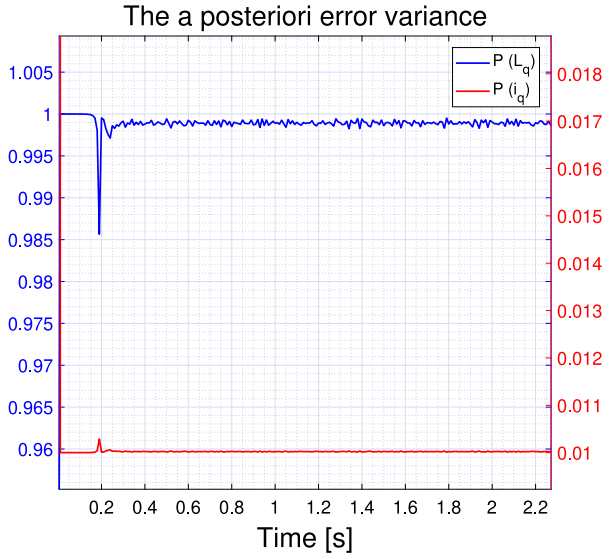

Fig. 15. A posteriori variance of i_q and L_q. (For interpretation of the references to color in this figure legend, the reader is referred to the web version of this article.)

References

[1] Yin S, Wang W. Study on the flux-weakening capability of permanent magnet synchronous motor for electric vehicle. Mechatronics 2016;38:115–20. http://dx.doi.org/10.1016/j.mechatronics.2016.03.005, URL https://www.sciencedirect.com/science/article/pii/S0957415816300095.

[2] Zhu M, Hu W, Kar NC. Acoustic noise-based uniform permanent-magnet demagnetization detection in SPMSM for high-performance PMSM drive. IEEE Trans Transp Electrif 2018;4(1):303–13. http://dx.doi.org/10.1109/TTE.2017.2755549.

[3] Li S, Han D, Sarlioglu B. Modeling of interior permanent magnet machine considering saturation, cross coupling, spatial harmonics, and temperature effects. IEEE Trans Transp Electrif 2017;3(3):682–93. http://dx.doi.org/10.1109/TTE.2017.2679212.

[4] Mercorelli P. Robust feedback linearization using an adaptive PD regulator for a sensorless control of a throttle valve. Mechatronics 2009;19(8):1334–45. http://dx.doi.org/10.1016/j.mechatronics.2009.08.008, URL https://www.sciencedirect.com/science/article/pii/S0957415809001512.

[5] Rinaldi G, Menon PP, Edwards C, Ferrara A. Sliding mode based dynamic state estimation for synchronous generators in power systems. IEEE Contr. Syst. Lett. 2018;2(4):785–90. http://dx.doi.org/10.1109/LCSYS.2018.2849585.

[6] Ghahremani E, Kamwa I. Dynamic state estimation in power system by applying the extended Kalman filter with unknown inputs to phasor measurements. IEEE Trans Power Syst 2011;26(4):2556–66. http://dx.doi.org/10.1109/TPWRS.2011.2145396.

[7] Bolognani S, Ortombina L, Tinazzi F, Zigliotto M. Model sensitivity of fundamental-frequency based position estimators for sensorless PM and reluctance synchronous motor drives. IEEE Trans Ind Electron 2018;65(1). http://dx.doi.org/10.1109/TIE.2017.2716902.

[8] De Soricellis M, Da Ru D, Bolognani S. A robust current control based on proportional-integral observers for permanent magnet synchronous machines. IEEE Trans Ind Appl 2018;54(2):1437–47. http://dx.doi.org/10.1109/TIA.2017.2772171.

[9] Hou Q, Ding S. Gpio based super-twisting sliding mode control for PMSM. IEEE Trans Circuits Syst II 2021;68(2):747–51. http://dx.doi.org/10.1109/TCSII.2020.3008188.

[10] Prakash A, Naveen C. Combined strategy for tuning sensor-less brushless DC motor using SEPIC converter to reduce torque ripple. ISA Trans 2022;133(2023):328–44. http://dx.doi.org/10.1016/j.isatra.2022.06.045.

[11] Leyva H, Aguirre-Hernández B, Espinoza JF. Stabilization of affine systems with polytopic control value sets. 2021, http://dx.doi.org/10.48550/ARXIV.2112.02451, URL https://arxiv.org/abs/2112.02451.

[12] Mercorelli P. A motion-sensorless control for intake valves in combustion engines. IEEE Trans Ind Electron 2017;64(4):3402–12. http://dx.doi.org/10.1109/TIE.2016.2598314.

[13] Yu Y, Huang X, Li Z, Wu M, Shi T, Cao Y, Yang G, Niu F. Full parameters estimation for permanent magnet synchronous motors. IEEE Trans Ind Electron 2021. http://dx.doi.org/10.1109/TIE.2021.3078391, 1–1.

[14] Ye S, Yao X. A modified flux sliding-mode observer for the sensorless control of PMSMs with online stator resistance and inductance estimation. IEEE Trans Power Electron 2020;35(8):8652–62. http://dx.doi.org/10.1109/TPEL.2019.2963112.

[15] Koteich M, Duc G, Maloum A, Sandou G. Observability of sensorless electric drives. 2018, arXiv e-prints, arXiv:1602.04468 arXiv:1602.04468.

[16] Vaclavek P, Blaha P, Herman I. AC drive observability analysis. IEEE Trans Ind Electron 2013;60(8):3047–59. http://dx.doi.org/10.1109/TIE.2012.2203775.

[17] Koteich M, Maloum A, Duc G, Sandou G. Discussion on AC drive observability analysis. IEEE Trans Ind Electron 2015;62(11):7224–5. http://dx.doi.org/10.1109/TIE.2015.2438777.

[18] Mercorelli P. An antisaturating adaptive preaction and a slide surface to achieve soft landing control for electromagnetic actuators. IEEE/ASME Trans Mechatronics 2010;17(1):76–85. http://dx.doi.org/10.1109/tmech.2010.2089467.

[19] Su Y, Zheng C, Mercorelli P. Nonlinear PD fault-tolerant control for dynamic positioning of ships with actuator constraints. IEEE/ASME Trans Mechatronics 2017;22(3):1132–42. http://dx.doi.org/10.1109/TMECH.2016.2603538.

[20] Schimmack M, Haus B, Mercorelli P. An extended Kalman filter as an observer in a control structure for health monitoring of a metal-polymer hybrid soft actuator. IEEE/ASME Trans Mechatronics 2018;23(3):1477–87. http://dx.doi.org/10.1109/TMECH.2018.2792321.

[21] Schimmack M, Poeschke F, Mercorelli P. Comparison of EKF and TSO for health monitoring of a textile based-heater structure and its control. IEEE/ASME Trans Mechatronics 2021;1–12. http://dx.doi.org/10.1109/TMECH.2021.3119097.

[22] Gan C, Chen Y, Sun Q, Si J, Wu J, Hu Y. A position sensorless torque control strategy for switched reluctance machines with fewer current sensors. IEEE/ASME Trans Mechatronics 2021;26(2):1118–28. http://dx.doi.org/10.1109/TMECH.2020.3017864.

[23] Chen H, Nie R, Gu J, Yan S, Zhao R. Efficiency optimization strategy for switched reluctance generator system with position sensorless control. IEEE/ASME Trans Mechatronics 2021;26(1):469–79. http://dx.doi.org/10.1109/TMECH.2020.3030001.

[24] Huo X, Wang B, Chen S, Chen W. Sensorless unbalance diagnosis of affiliated rotating chamber based on driving current of permanent magnet synchronous motor. IEEE/ASME Trans Mechatronics 2021;26(6):2899–909. http://dx.doi.org/10.1109/TMECH.2020.3048378.

[25] Meessen KJ, Thelin P, Soulard J, Lomonova EA. Inductance calculations of permanent-magnet synchronous machines including flux change and self- and cross-saturations. IEEE Trans Magn 2008;44(10):2324–31. http://dx.doi.org/10.1109/TMAG.2008.2001419.

[26] Lee J-Y, Lee S-H, Lee G-H, Hong J-P, Hur J. Determination of parameters considering magnetic nonlinearity in an interior permanent magnet synchronous motor. IEEE Trans Magn 2006;42(4):1303–6. http://dx.doi.org/10.1109/TMAG.2006.871951.

[27] Boileau T, Leboeuf N, Nahid-Mobarakeh B, Meibody-Tabar F. Online identification of PMSM parameters: Parameter identifiability and estimator comparative study. IEEE Trans Ind Appl 2011;47(4):1944–57. http://dx.doi.org/10.1109/TIA.2011.2155010.

[28] Lai C, Feng G, Mukherjee K, Loukanov V, Kar NC. Torque ripple minimization for interior PMSM with consideration of magnetic saturation incorporating online parameter identification. IEEE Trans Magn 2017;53(6):1–4. http://dx.doi.org/10.1109/TMAG.2017.2666089.

[29] Yao Y, Huang Y, Peng F, Dong J, Zhu Z. Compensation method of position estimation error for high-speed surface-mounted PMSM drives based on robust inductance estimation. IEEE Trans Power Electron 2022;37(2):2033–44. http://dx.doi.org/10.1109/TPEL.2021.3106510.

[30] Feng G, Lai C, Kar NC. A novel current injection-based online parameter estimation method for PMSMs considering magnetic saturation. IEEE Trans Magn 2016;52(7):1–4. http://dx.doi.org/10.1109/TMAG.2016.2525805.

[31] Gan H, Cao Z, Chen P, Luo Y, Luo X. Fractional-order electromagnetic modeling and identification for PMSM servo system. ISA Trans 2024;147:527–39. http://dx.doi.org/10.1016/j.isatra.2024.01.036, URL https://www.sciencedirect.com/science/article/pii/S0019057824000466.

[32] Luca M, Azou S, Burel G, Serbanescu A. On exact Kalman filtering of polynomial systems. IEEE Trans Circuits Syst I 2006;53(6):1329–40. http://dx.doi.org/10.1109/TCSI.2006.870899.

[33] Müller P, Weber H. Analysis and optimization of certain qualities of controllability and observability for linear dynamical systems. Automatica 1972;8(3):237–46. http://dx.doi.org/10.1016/0005-1098(72)90044-1.

[34] Krener AJ, Ide K. Measures of unobservability. In: Proceedings of the 48h IEEE conference on decision and control (CDC) held jointly with 2009 28th Chinese control conference. 2009, p. 6401–6. http://dx.doi.org/10.1109/CDC.2009.5400067.

[35] Zwerger T, Mercorelli P. Using a bivariate polynomial in an EKF for state and inductance estimations in the presence of saturation effects to adaptively control a PMSM. IEEE Access 2022;10:111545–53. http://dx.doi.org/10.1109/ACCESS.2022.3215511.

[36] Zwerger T, Mercorelli P. Backward extended Kalman filter to estimate and adaptively control a PMSM in saturation conditions. IEEE J Emerg Sel Top Ind Electron 2024;5(2):462–74. http://dx.doi.org/10.1109/JESTIE.2023.3313066.

[37] Zhu ZQ, Liang D, Liu K. Online parameter estimation for permanent magnet synchronous machines: An overview. IEEE Access 2021;9:59059–84. http://dx.doi.org/10.1109/ACCESS.2021.3072959.

[38] jie Wu Y, fei Li G. Adaptive disturbance compensation finite control set optimal control for PMSM systems based on sliding mode extended state observer. Mech Syst Signal Process 2018;98:402–14. http://dx.doi.org/10.1016/j.ymssp.2017.05.007, URL https://www.sciencedirect.com/science/article/pii/S0888327017302601.

[39] Kannan R, Rajasekaran S, Stallon SD, Anand R. Improved indirect instantaneous torque control based torque sharing function approach of SRM drives in EVs using hybrid technique. ISA Trans 2023. http://dx.doi.org/10.1016/j.isatra.2023.04.001.

[40] Zhang Q, Guo H, Liu Y, Guo C, Lu K, Wang D, Zhang Z, Sun J. Robust plug-in repetitive control for speed smoothness of cascaded-PI PMSM drive. Mech Syst Signal Process 2021;163(2022):108090. http://dx.doi.org/10.1016/j.ymssp.2021.108090.

[41] Hassan M, Ge X, Woldegiorgis AT, Mastoi MS, Shahid MB, Atif R, Shaikh MS, Kumar S. A look-up table-based model predictive torque control of IPMSM drives with duty cycle optimization. ISA Trans 2023. http://dx.doi.org/10.1016/j.isatra.2023.02.007.

[42] Liang W, Zhao W, Wang C, Zou S. Harmonic suppression and road feeling control of steer-by-wire system with permanent magnet synchronous motor. Mech Syst Signal Process 2022;172:108983. http://dx.doi.org/10.1016/j.ymssp.2022.108983.

[43] Yao Y, Lin J, Zhang B, Jiang D, Chen L. Improved strong tracking extended Kalman filter for identifying load disturbances and model uncertainties of serial–parallel mechanism. Mech Syst Signal Process 2022;171:108819. http://dx.doi.org/10.1016/j.ymssp.2022.108819.

[44] Ortega R, Monshizadeh N, Monshizadeh P, Bazylev D, Pyrkin A. Permanent magnet synchronous motors are globally asymptotically stabilizable with PI current control. Automatica 2018;98:296–301. http://dx.doi.org/10.1016/j.automatica.2018.09.031, URL https://www.sciencedirect.com/science/article/pii/S0005109818304564.

[45] Sun Y, Zhu J, Fu C, Chen Z. Decoupling control of cascaded power electronic transformer based on feedback exact linearization. IEEE J Emerg Sel Top Power Electron 2022;10(4):3662–76. http://dx.doi.org/10.1109/JESTPE.2021.3069208.

[46] Moore B. Principal component analysis in linear systems: Controllability, observability, and model reduction. IEEE Trans Autom Control 1981;26(1):17–32. http://dx.doi.org/10.1109/TAC.1981.1102568.

[47] Nalepa R, Orlowska-Kowalska T. Optimum trajectory control of the current vector of a nonsalient-pole PMSM in the field-weakening region. IEEE Trans Ind Electron 2012;59(7):2867–76. http://dx.doi.org/10.1109/TIE.2011.2116755.

[48] B M, et al. Solving polynomial equations: foundations, algorithms, and applications. New Jersey-USA: Springer; 2006.

[49] Basile G, Marro G. Controlled and conditioned invariants in linear system theory. New Jersey-USA: Prentice Hall; 1992.

[50] Slotine J-JE, Li W. Applied nonlinear control. Pearson Education Taiwan; 1991.

[51] Typhoon HIL for high-fidelity EV and e-mobility. 2022, https://www.typhoon-hil.com/solutions/e-mobility/. [Accessed 19 January 2022].

[52] Kim K-C. A novel method for minimization of cogging torque and torque ripple for interior permanent magnet synchronous motor. IEEE Trans Magn 2014;50(2):793–6. http://dx.doi.org/10.1109/TMAG.2013.2285234.

[53] Kim HM, Kim Y-J, Jung S-Y. Torque ripple and back emf harmonic reduction of IPMSM with asymmetrical stator design. In: 2017 20th international conference on electrical machines and systems. ICEMS, 2017, p. 1–4. http://dx.doi.org/10.1109/ICEMS.2017.8056477.

[54] Hilairet M, Auger F, Berthelot E. Speed and rotor flux estimation of induction machines using a two-stage extended Kalman filter. Automatica 2009;45(8):1819–27. http://dx.doi.org/10.1016/j.automatica.2009.04.005.

[55] Mercorelli P. A two-stage augmented extended Kalman filter as an observer for sensorless valve control in camless internal combustion engines. IEEE Trans Ind Electron 2012;59(11):4236–47.

[56] Zwerger T, Mercorelli P. Dual Kalman filters analysis for interior permanent magnet synchronous motors. In: Bartoszewicz A, Kabziński J, Kacprzyk J, editors. Advanced, contemporary control. Cham: Springer International Publishing; 2020, p. 424–35.

[57] Butcher J. Numerical methods for ordinary differential equations. Wiley; 2003, http://dx.doi.org/10.1002/0470868279.

[58] Hermann R, Krener A. Nonlinear controllability and observability. IEEE Trans Autom Control 1977;22(5):728–40. http://dx.doi.org/10.1109/TAC.1977.1101601.

[59] Zwerger T, Mercorelli P. Optimal control strategies for PMSM with a decoupling super twisting smc and inductance estimation in the presence of saturation. J Frank Inst 2024;361(11):106934. http://dx.doi.org/10.1016/j.jfranklin.2024.106934, URL https://www.sciencedirect.com/science/article/pii/S0016003224003557.

[60] Rezaei V, Stefanovic M. Distributed decoupling of linear multiagent systems with interconnected nonlinear uncertainties. In: 2016 IEEE 55th conference on decision and control. CDC, 2016, p. 5232–7. http://dx.doi.org/10.1109/CDC.2016.7799070.

[61] Liu K, Wang S, Liang H, Shi Z, Li M, Yu C, Zhou K, Gong X, Yuan G, Qi C. Improved feature decoupling transfer network modeling based on singular value decomposition for SOC estimation in energy-storage lithium-ion batteries. J Electrochem Soc 2023;170(7):070521. http://dx.doi.org/10.1149/1945-7111/ace65b.

[62] Wang W, Mu J. State of charge estimation for lithium-ion battery in electric vehicle based on Kalman filter considering model error. IEEE Access 2019;7:29223–35. http://dx.doi.org/10.1109/ACCESS.2019.2895377.

[63] Liu K, Liu Y, Song F, Tan J. Data-driven calibration of decoupling matrix for MIMO precision motion stages. ISA Trans 2024;150:223–31. http://dx.doi.org/10.1016/j.isatra.2024.05.002, URL https://www.sciencedirect.com/science/article/pii/S0019057824002052.

[64] Welch G, Bishop G. An introduction to the Kalman filter. Prentice Hall, Chapel Hill, NC, USA: Univ. North Caroline Chapel Hill; 1995.